

A Hurricane Boundary Layer and Wind Field Model for Use in Engineering Applications

PETER J. VICKERY AND DHIRAJ WADHERA

Applied Research Associates, Inc., Raleigh, North Carolina

MARK D. POWELL

NOAA/AOML/Hurricane Research Division, Miami, Florida

YINGZHAO CHEN

Applied Research Associates, Inc., Raleigh, North Carolina

(Manuscript received 27 July 2007, in final form 29 July 2008)

ABSTRACT

This article examines the radial dependence of the height of the maximum wind speed in a hurricane, which is found to lower with increasing inertial stability (which in turn depends on increasing wind speed and decreasing radius) near the eyewall. The leveling off, or limiting value, of the marine drag coefficient in high winds is also examined. The drag coefficient, given similar wind speeds, is smaller for smaller-radius storms; enhanced sea spray by short or breaking waves is speculated as a cause. A fitting technique of dropsonde wind profiles is used to model the shape of the vertical profile of mean horizontal wind speeds in the hurricane boundary layer, using only the magnitude and radius of the “gradient” wind. The method slightly underestimates the surface winds in small but intense storms, but errors are less than 5% near the surface. The fit is then applied to a slab layer hurricane wind field model, and combined with a boundary layer transition model to estimate surface winds over both marine and land surfaces.

1. Introduction

A hurricane boundary layer model is developed using a combination of mean profiles of horizontal wind speed computed using dropsonde data and a linear theoretical hurricane boundary layer model developed by Kepert (2001). The final hurricane boundary layer model incorporates a combined logarithmic–quadratic variation of the mean wind speed with height used to replicate the height of the low-level jet observed in the hurricane boundary layer. The empirical hurricane boundary layer model reproduces the shape of the hurricane boundary layer over the lower 1000 m. The analysis of the vertical profiles of wind speed from dropsonde data reproduces the observations noted in Powell et al. (2003) that the sea drag coefficient reaches a maximum value. The results also suggest that the magnitude of this maximum

decreases with decreasing storm radius to maximum winds (RMW).

A simple linear regression model is used to determine the depth of the boundary layer, which, as predicted by Kepert (2001), decreases with an increase in the inertial stability parameter. The change in the height of the boundary layer as the wind moves from the sea to the land was modeled using the approach outlined in Kepert (2001), and is coupled with a traditional approach to model the reduction in the wind speed from sea to land. The results suggest that the reduction in the wind speed associated with the sea–land transition varies with the height of the hurricane boundary layer, and consequently, varies with storm size and intensity because of the relationship between the boundary layer height and the inertial stability parameter.

The hurricane boundary layer model is coupled with a slab representation of a hurricane and validated through comparisons of modeled and observed peak gust wind speeds measured at both open water and overland locations. The comparisons suggest that the model

Corresponding author address: Peter J. Vickery, 8540 Colonnade Center Drive, Suite 307, Raleigh, NC 27615.
E-mail: pvickery@ara.com

adequately reproduces the key characteristics of the hurricane boundary layer and the transition from sea to land.

2. Analysis of dropsonde data

Dropsondes are dropped from reconnaissance aircraft generally from heights between 1.5 and 3 km. Dropsondes fall vertically downward at speeds of about 10 m s^{-1} measuring wind speed, temperature, humidity, and so on, every 0.5 s. Dropsondes hit the sea surface after several minutes from the time of drop, drifting 10–15 km tangentially and hundreds of meters radially (Powell et al. 2003). Further dropsonde details are given in Hock and Franklin (1999) and Franklin et al. (2003). The dropsonde dataset used here was obtained from the Atlantic Oceanographic and Meteorological Laboratories Hurricane Research Division (AOML HRD) and consists of all vertical profiles of wind speed collected during the 1997–2003 hurricane seasons. Most of these profiles are from Atlantic Ocean and Gulf of Mexico hurricanes with a few coming from Pacific Ocean hurricanes. The dropsonde data has been previously subjected to a quality control criterion by AOML HRD to remove any identifiable errors. All measurements have been smoothed by AOML HRD using a 5-s low-pass filter to remove noise due to switching of the satellites.

The dropsondes were separated into two groups associated with (i) vertical profiles measured at or near the radius to maximum winds and (ii) with drops away from the RMW. The assignment of a particular vertical profile of horizontal wind speed to either the RMW region or the outer vortex region was determined using comments of the flight meteorologist, an examination of concurrent flight-level radial wind profiles (if available), airborne radar reflectivity imagery, and H*Wind (Powell et al. 1996, 1998) objective wind field analyses. Following the approach of Powell et al. (2003), the vertical profiles of wind speed were analyzed in a composite sense, as a function of the mean boundary layer (MBL) wind speed, defined as the mean wind speed averaged over a height range of 10 to 500 m. The six different mean boundary layer wind speed groups correspond to 20–29, 30–39, 40–49, 50–59, 60–69, and 70–85 m s^{-1} . Each group was divided vertically into height bins chosen to provide maximum resolution close to the sea surface. In the mean boundary layer wind speed averaging process, we assume [consistent with Powell et al. (2003)] that the wind speed samples from the dropsondes are from a stationary and ergodic process. Thus the effective averaging time of the final vertical profile of horizontal wind speeds is consistent with a time scale long enough to filter out the turbulent features within the boundary layer (i.e., times

scales shorter than that associated with the spectral gap). Thus, the effective averaging time is representative of durations of the order of ~ 10 to ~ 60 min, and throughout this article, the term mean wind speed is taken to be representative of time scales of the order of 10 min or longer. The mean wind speeds versus height were computed by taking the average of all wind speed measurements within height bins of 10 m for heights less than 300 m, 20 m bins for heights ranging between 300 and 500 m, 50 m bins for heights between 500 and 1000 m, and 100-m bins for heights greater than 1000 m. The single height value assigned to each bin is the mean value computed within height bin. Table 1 presents a summary of the number of vertical profiles of wind speed in each mean boundary layer wind speed group for each of the hurricanes analyzed. Two sets of radii groups were developed. The first group consists of drops performed at or near the radius to maximum winds, and the second group consists of drops performed outside of the RMW. Tables 2 and 3 present the number of dropsonde profiles in each of the mean boundary layer wind speed and radial group combinations.

Figure 1 shows the vertical profiles of the mean horizontal wind speed near the RMW for each of the six mean boundary layer wind speed groups. Qualitatively, Fig. 1 indicates that in the lower few 100 m of the boundary layer, the variation of the mean wind speed with height is approximately logarithmic, and the height at which the maximum wind speed occurs decreases with increasing wind speed. The height maxima range from a maximum of about 700 m for the 20–29 m s^{-1} mean boundary layer wind speed case, to a minimum of about 400 m for the 60–69 m s^{-1} mean boundary layer wind speed case.

The lowering of the height at which the maximum wind speed occurs is consistent with the analysis described in Kepert (2001) and Kepert and Wang (2001), where the existence of a lower level “jet” is discussed. The jet strength is defined as the ratio of the maximum wind speed divided by the gradient balance wind speed. Kepert considers the jet height to be equivalent to the boundary layer height, and that concept is carried through here. Kepert (2001) demonstrates that both the magnitude and height of the jet are a function of the inertial stability I , defined as

$$I = \sqrt{\left(f + \frac{2V}{r}\right)\left(f + \frac{V}{r} + \frac{\partial V}{\partial r}\right)}, \quad (1)$$

where V is the azimuthally averaged tangential gradient wind speed (as computed from the surface pressure field), f is the Coriolis parameter, and r is the radial

TABLE 1. Number of profiles by hurricane and mean boundary layer wind speed range.

Storm name	Year	Mean boundary layer wind speed range (m s ⁻¹)						
		All	20–29	30–39	40–49	50–59	60–69	70–85
Barry	2001	3		2				1
Bill	2003	2	2					
Bonnie	1998	71	9	27	26	9		
Bret	1999	27	8	4	3	5	5	2
Chantal	2001	6	5	1				
Claudette	2003	20	12	8				
Danielle	1998	37	22	14	1			
Debby	2000	2		2				
Dennis	1999	56	19	20	15	2		
Earl	1998	6	5	1				
Erika	1997	16	16					
Erin	2001	7		2		4		1
Fabian	2003	89	4	22	16	30	15	2
Florence	2000	13	3	2			6	2
Floyd	1998	63	5	5	30	20	3	
Gabrielle	2001	7	7					
Georges	1998	50	11	15	12	8	3	1
Gert	1999	7		2	1	2	2	
Gordon	2000	2	2					
Gustav	2002	18	9	5	4			
Helene	2000	6	6					
Humberto	2001	74	51	12	10		1	
Irene	1999	20	18	2				
Iris	2001	13	5			1		7
Isabel	2003	88	5	23	31	10	7	12
Isidore	2002	65	18	14	10	14	6	3
Jose	1999	3	3					
Keith	2000	5	3		1	1		
Larry	2003	1	1					
Lenny	1999	14	5	4	3	1	1	
Lili	2002	32	1	11	5	8	3	4
Michael	2000	17	14	2				1
Michelle	2001	25	4	4	6	6	5	
Mitch	1998	28	3	6	2	4	7	6
Odette	2003	3	3	3				

TABLE 2. Number of profiles near the RMW.

Radius range (km)	Mean boundary layer wind speed range (m s ⁻¹)					
	20–29	30–39	40–49	50–59	60–69	70–85
All	209	136	146	91	43	25
10–30	87	36	39	49	24	12
30–60	60	48	42	26	19	13
60–100	62	52	65	16		

The friction velocity is related to the surface shear stress (τ) as

$$\tau = \rho u_*^2 = \rho C_d U_{10}^2, \quad (3)$$

where C_d is the surface drag coefficient, ρ is the density of air, and U_{10} is the mean wind speed (representative of the wind speed averaged over a period of 10 min to 1 h) at a height of 10 m.

For each combination of r and mean boundary layer wind speed, an estimate of the surface roughness and sea surface drag coefficient was obtained using a least squares fit (in linear-logarithmic space, referred to as LSF) of the measured wind speeds over height ranges of 20–200, 20–150, and 20–100 m (Fig. 2). A lower bound of 20 m is chosen because of the scarcity of observational data in the lower 10 m. Tables 4 and 5 provide the number of observations for each mean boundary layer wind speed range and height bin for the near RMW and outside RMW vertical profiles of the mean horizontal wind speed, respectively. The vertical profiles of the mean horizontal wind speed given in Fig. 2 show a trend for the height of the mean horizontal wind speed maxima to decrease as both the RMW decreases and the wind speed increases, consistent with the

distance from the center of the storm. As indicated in (1), the inertial stability factor is a function of both wind speed and radius, and thus to take into account the effect of radius, the dropsonde data were further divided into bins having similar values of r .

As in Powell et al. (2003) for a neutrally stable boundary layer, the vertical variation in the mean wind speed with height near the surface is controlled by the surface roughness and is given by

$$U(z) = \frac{u_*}{k} \ln\left(\frac{z}{z_0}\right), \quad (2)$$

where k is the von Kármán coefficient having a value of 0.4, u_* is the friction velocity, z is the height above the ground, and z_0 is the surface roughness.

TABLE 3. Number of profiles N outside the RMW.

Mean boundary layer wind speed range (m s ⁻¹)	Radius range (km)	N
20–29	All	72
20–29	40–80	26
20–29	85–105	24
20–29	105–150	22
30–39	All	74
30–39	30–65	24
30–39	65–105	25
30–39	105–150	25
40–49	All	30
40–49	30–90	20
40–49	90–150	10
50–59	All	34
50–59	30–50	16
50–59	50–150	18
60–69	50–75	22

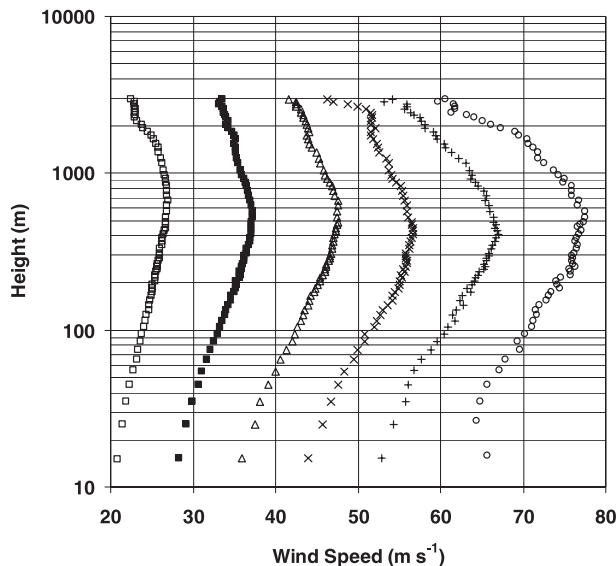


FIG. 1. Mean wind profiles near the RMW: 20–29, 30–39, 40–49, 50–59, 60–69, and 70–85 m s^{-1} .

analysis of Kepert (2001). Using the intercepts from the least squares fits, estimates of the mean wind speed at 10 m U_{10} and the effective surface roughness z_0 (ranging from 0.001 to 0.003 m), and the associated uncertainty were obtained for each wind speed profile. Using the estimated value of z_0 , the surface drag coefficient is computed using Eqs. (2) and (3).

Figure 3 presents the resulting C_d versus U_{10} data for the three LSF height ranges. Results are given both for the mean boundary layer wind speed data separated by RMW bins, and with no separation by RMW (as in Powell et al. 2003). The 95% confidence bounds shown in Fig. 3 represent a lower bound because the error in the intercept does not include any errors associated with the estimates of the dropsonde height z nor the errors in the estimates of the measured wind speed at each height. As seen in Fig. 3, on average, the drag coefficient increases with increasing wind speed up to wind speeds of about 24–28 m s^{-1} and then starts to level off or perhaps even decrease for higher wind speeds, consistent with the results of Powell et al. (2003). The data suggest that the magnitude of the maximum value of C_d decreases with decreasing RMW. Also shown in Fig. 3 is the Large and Pond (1981) drag coefficient model, modified to have a maximum value that varies with the RMW. The maximum (cap) values range from 0.0019 for the smallest storms up to 0.0024 for the largest storms.

The approach taken for examining the characteristics of the hurricane boundary layer near the RMW was repeated for dropsonde profiles measured outside the RMW. The radius groups chosen were determined based on the

number of vertical profiles of horizontal wind speed associated within each mean boundary layer wind speed group. Figure 4 shows the resulting mean wind speed profiles along with the logarithmic fits to the wind speed data over the 20–200-m range. As indicated in Fig. 4, there is a trend for the height of the wind maxima to increase as the radius increases and decrease with an increase in wind speed, again consistent with Kepert (2001).

Figure 5 shows a comparison of the estimated values of C_d and the error bounds corresponding to a 95% confidence interval plotted versus U_{10} . On average, the drag coefficient increases with increasing wind speed up to about 30 m s^{-1} and then levels off, but the apparent decrease in C_d at higher wind speeds evident in the case of the near RMW observations is not evident here.

To incorporate the effect of radius on the limiting value of C_d , the limiting value of C_d is modeled as a function of radius, r in the form:

$$C_{d_{\max}} = (0.0881r + 17.66)10^{-4},$$

$$0.0019 \leq C_{d_{\max}} \leq 0.0025, \quad (4)$$

where r is the radial distance from the storm center (km), but r is constrained to have a minimum value equal to the RMW.

A possible explanation for the reduction in C_d as a function of radius is given in Makin (2005) where it is suggested that a limiting value of C_d is caused by the production of sea spray inhibiting the transfer of momentum from the wind to the sea surface. Makin suggests that most of the sea spray is produced by the mechanical tearing by the wind from steep short waves, and thus for storms with small RMW (and hence small wind fetches) more of the waves will be short as compared with the large RMW case. Bye and Jenkins (2006) also attempt to explain the limiting C_d phenomenon through the modeling of sea spray effects in a model for C_d .

Although the mean wind speed profile is well described by a simple log law over a height range of ~20–300 m, in some of the high wind speed cases, the mean wind speeds near the surface determined from the dropsondes began to deviate from the log law (see Figs. 1, 2, 4, and 6). It is not clear whether this deviation is real or is an artifact of the much smaller number of samples in the lower height ranges as compared with the higher heights. This difference in modeled and observed wind speeds near the surface is worthy of further study, and could be a result of a “slip” surface produced by sea spray or bubbles, inhibiting momentum transfer at the air–sea interface.

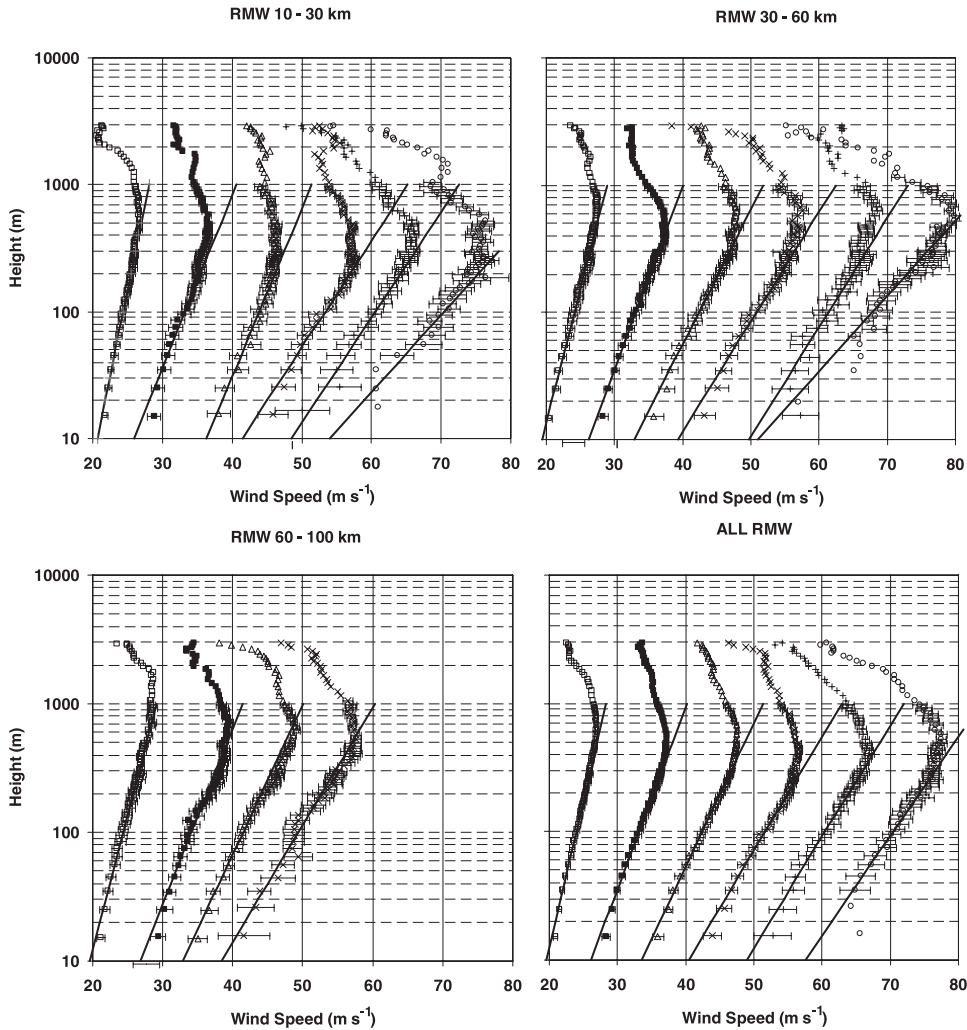


FIG. 2. Mean and fitted logarithmic profiles near the RMW for all mean boundary layer wind speed cases. Horizontal error bars represent the 95th percentile error on the estimate of the mean wind speed. Least squares fits are for the 20–200-m case. MBL cases correspond to 20–29, 30–39, 40–49, 50–59, 60–69, and 70–85 m s^{-1} .

3. Empirical model for the marine hurricane boundary layer

In the lower few 100 m, the atmospheric boundary layer of the hurricane is adequately modeled using the logarithmic law; however, the wind speed profiles shown in Figs. 2 and 4 clearly indicate that in some cases such a model can be used well beyond heights of about 300 m. As height is increased, the applicability of the logarithmic law breaks down and the wind speeds begin to decrease with increasing height. The height at which the logarithmic law fails to describe the variation of the mean horizontal wind speed with height is strongly correlated with the height at which the mean horizontal wind speed reaches a maximum value (i.e.,

jet or boundary layer height). With this observation noted, the hurricane boundary layer was modeled in the form

$$U(z) = \frac{u_*}{k} \left[\ln\left(\frac{z}{z_0}\right) - a\left(\frac{z}{H^*}\right)^n \right]. \quad (5)$$

Each of the parameters a and n were treated as free parameters but were required to be constant for all values of r and H^* (boundary layer height parameter). The boundary layer, or jet height, was allowed to vary with each vertical profile of the mean horizontal wind speed. To determine the appropriate parameters

TABLE 4. Number of observations by MBL range and height bin for near RMW profiles.

Height bin center (m)	Mean boundary layer wind speed 20–29 m s ⁻¹	Mean boundary layer wind speed 30–39 m s ⁻¹	Mean boundary layer wind speed 40–49 m s ⁻¹	Mean boundary layer wind speed 50–59 m s ⁻¹	Mean boundary layer wind speed 60–69 m s ⁻¹	Mean boundary layer wind speed 70–85 m s ⁻¹
5	11	7	11	3	1	1
15	297	182	134	53	14	2
25	295	181	159	73	21	1
35	308	212	175	97	27	4
45	319	211	175	101	33	6
55	323	202	197	102	40	14
65	328	221	197	110	37	19
75	331	212	200	101	42	22
85	339	213	203	109	45	19
95	312	208	203	101	55	23
105	337	221	215	102	49	26
115	324	215	202	114	58	29
125	331	207	211	120	59	28
135	333	218	221	124	55	33
145	322	215	207	122	47	34
155	321	222	199	120	58	31
165	338	200	202	119	55	27
175	320	221	210	118	55	33
185	321	210	212	134	58	32
195	330	215	199	131	61	36
205	338	212	208	122	58	35
215	326	213	208	141	58	31
225	323	215	218	127	58	31
235	326	217	199	135	61	37
245	321	214	220	128	56	35
255	309	231	212	140	62	32
265	335	220	204	134	53	38
275	324	226	213	128	55	39
285	317	229	200	136	58	38
295	311	220	215	126	50	38
310	632	444	411	266	121	80
330	645	436	405	271	119	73
350	636	437	409	269	112	62
370	617	428	401	267	103	71
390	650	426	413	258	108	76
410	641	434	411	279	119	84
430	644	416	402	265	107	75
450	615	433	420	255	104	81
470	627	430	430	258	117	71
490	637	428	394	260	109	69
525	1570	1077	1048	646	283	175
575	1551	1054	1012	665	282	146
625	1546	1041	1047	656	266	129
675	1528	1023	1027	650	270	147
725	1482	1025	1013	651	285	152
775	1435	1002	995	643	282	163
825	1454	987	953	646	304	179
875	1422	961	947	628	290	156
925	1400	926	937	600	290	172
975	1381	930	918	573	281	188

for use in Eq. (5), two approaches were taken, as follows.

Method 1: The values of u_* and z_0 were computed from the regression analysis and the values of a , n ,

and H^* were selected to minimize the error over the height range of 20 to 1000 m.

Method 2: The values of z_0 were computed using the capped Large and Pond (1981) drag coefficient model and the values of u_* , a , n , and H^* were

TABLE 5. Number of observations by MBL range and height bin for outside-RMW profiles.

Height bin center (m)	Mean boundary layer wind speed 20–29 m s ⁻¹	Mean boundary layer wind speed 30–39 m s ⁻¹	Mean boundary layer wind speed 40–49 m s ⁻¹	Mean boundary layer wind speed 50–59 m s ⁻¹	Mean boundary layer wind speed 60–69 m s ⁻¹	Mean boundary layer wind speed 70–85 m s ⁻¹
5	4	2	1	1	2	1
15	75	74	28	8	5	1
25	74	79	36	18	12	4
35	83	89	43	23	14	4
45	79	86	44	30	13	4
55	83	94	49	28	17	7
65	75	100	45	33	27	6
75	79	101	48	31	34	10
85	77	99	46	31	31	11
95	82	100	57	36	37	12
105	81	89	53	36	26	12
115	74	96	46	38	31	12
125	74	99	50	33	33	12
135	79	97	49	40	27	12
145	74	101	52	38	29	13
155	76	95	49	39	25	17
165	75	96	53	34	26	17
175	77	103	53	36	28	20
185	71	95	50	36	31	17
195	74	101	59	37	29	22
205	82	107	49	36	35	21
215	76	98	53	37	37	20
225	81	99	53	37	34	22
235	85	100	58	37	32	23
245	78	92	51	42	33	18
255	85	103	52	36	35	23
265	83	99	56	36	38	24
275	91	94	49	38	33	23
285	78	88	57	33	35	26
295	83	96	49	39	32	20
310	166	196	103	68	67	39
330	172	205	104	74	72	54
350	160	202	103	74	69	51
370	167	201	104	79	72	43
390	160	200	106	66	72	42
410	158	197	102	70	70	40
430	154	198	101	73	70	41
450	158	197	106	73	75	36
470	160	192	101	76	77	36
490	168	189	109	74	83	42
525	393	499	260	197	176	108
575	399	490	265	189	167	95
625	394	474	257	198	190	111
675	387	474	251	185	187	109
725	386	452	243	193	178	99
775	392	467	240	196	170	110
825	378	450	242	197	161	110
875	373	442	233	184	161	103
925	385	415	236	176	165	102
975	377	398	222	194	159	108

selected to minimize the error over the height range of 20 to 1000 m.

Figure 6 presents the observed and modeled mean wind speed profiles near the RMW for the 10–30- and

30–60-km RMW cases. Table 6 presents the values of H^* , U_{10} , C_d , z_0 , and the resulting R^2 values computed over the 20–1000-m height range for all RMW ranges. In all cases, the best values of a and n were 0.4 and 2.0, respectively. By setting the derivative of Eq. (5) with

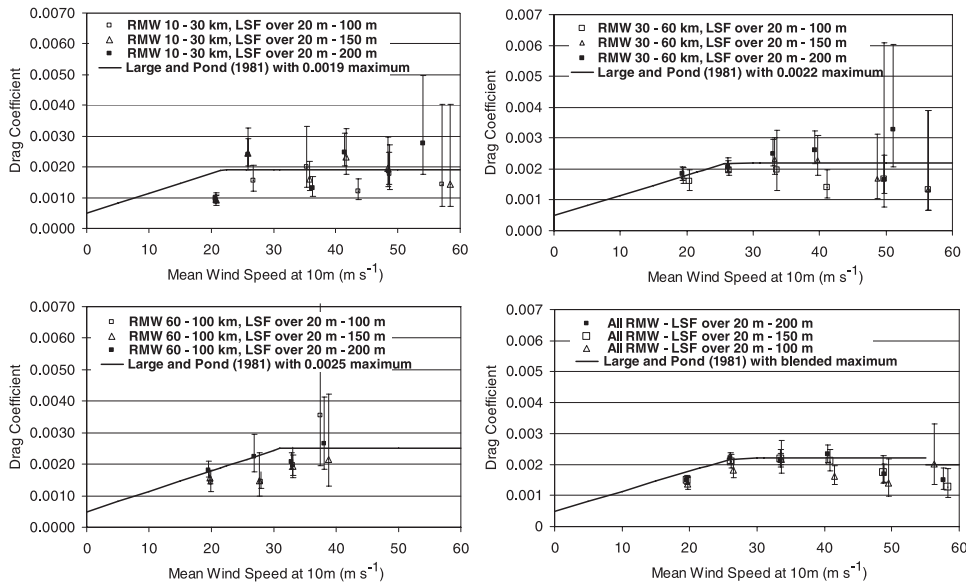


FIG. 3. Variation of the sea surface drag coefficient with mean wind speed at 10 m, near the RMW.

respect to z equal to zero it is seen that the boundary layer or jet height H is equal to $1.12H^*$. Table 7 presents the values of H^* , U_{10} , C_d , z_0 , and the resulting R^2 values computed over a height range of 20–1000 m for the boundary layer outside the RMW. Alternate models for the boundary layer such as that given in Kepert (2001) could also be used in lieu of Eq. (5); however, Eq. (5) has the advantage that the form of the model is consistent with the well-used log law.

a. Hurricane boundary layer height

According to Kepert (2001), the jet height or boundary layer height H is inversely proportional to \sqrt{I} and is given as

$$H = \sqrt{\frac{2K}{I}} \tan^{-1} \left(-1 - \frac{2}{\chi} \right), \quad \text{where} \quad (6a)$$

$$\chi = C_d V \sqrt{\frac{2}{KI}}, \quad (6b)$$

where K is the turbulent diffusivity of momentum, I is inertial stability, V is the gradient wind speed, and C_d is the surface drag coefficient.

Here, the boundary layer height is also modeled as a function of I , where in the calculation of I an average value of the radius within a radius bin is used to define r , the maximum wind speed from the mean horizontal wind speed profile is used as a surrogate for the gradient velocity V and the $\partial V/\partial r$ term in Eq. (1) is neglected. Using the estimates of the boundary layer height, H^* for

r both near and outside the RMW, regression models relating H^* and I are given by

$$H^* = 343.7 + 0.260/I \quad R^2 = 0.75, \quad \sigma_e = 99 \text{ m} \quad (7a)$$

$$H^* = 186.6 + 12.66/\sqrt{I} \quad R^2 = 0.70, \quad \sigma_H = 106 \text{ m}. \quad (7b)$$

The regression model for H^* modeled as a function of $1/I$ explains 75% of the variance associated with the underlying data, whereas when H^* is modeled as a function of $1/\sqrt{I}$ the model explains 70% of the variance. The boundary layer height model is in general agreement with Kepert’s (2001) analysis, where the boundary layer height scaling parameter was shown to be inversely proportional to the square root of the inertial stability. Based on the observed values of H^* , the model values of H^* are capped using a lower bound of 300 m and an upper bound of 1200 m.

Figure 7 shows a comparison of the H^* derived from the regression models H derived using Eq. (6) with $K = 75 \text{ m}^2 \text{ s}^{-1}$ (Kepert 2001) and the observed values of H^* . Note that the use of a constant value of K in Eq. (6) is a simplification of the theory in Kepert (2001).

b. Marine boundary layer model verification

Using Eqs. (3) and (5) to define the variation of the mean horizontal wind speed with height, coupled with Eq. (7a) to define the boundary layer height, the characteristics of the boundary layer were estimated given only U_{max} and r . In the verification process, the value of

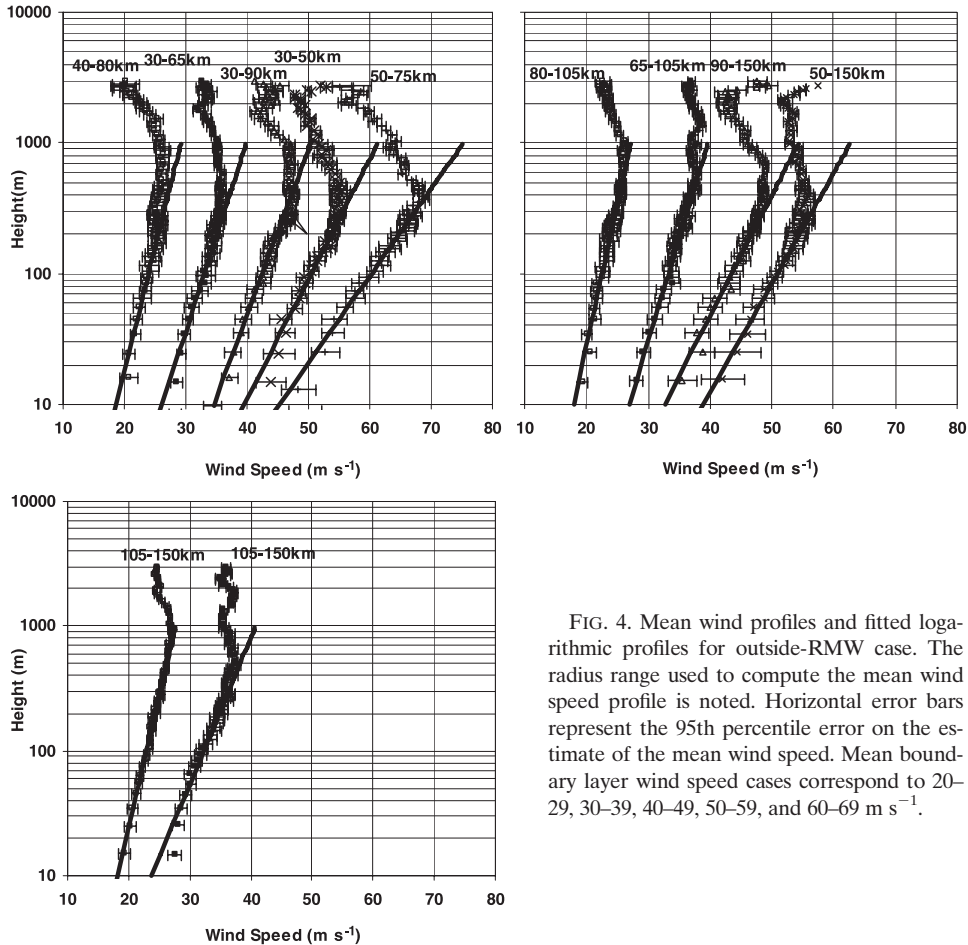


FIG. 4. Mean wind profiles and fitted logarithmic profiles for outside-RMW case. The radius range used to compute the mean wind speed profile is noted. Horizontal error bars represent the 95th percentile error on the estimate of the mean wind speed. Mean boundary layer wind speed cases correspond to 20–29, 30–39, 40–49, 50–59, and 60–69 $m s^{-1}$.

U_{max} is set equal to the maximum mean wind speed obtained by the dropsondes over the range of 20–1000 m, and r is equal to the mean value of r used to determine the RMW or r bin.

Figure 8 presents examples of the modeled and observed boundary layer wind speed profiles for the 10–30- and 30–60-km RMW cases. Figure 9 shows the mean and coefficient of variation (CoV) of the error plotted versus height (with the errors computed over ranges of heights) where it is seen that in most cases the error is less than 5%; however, there is a weak trend evident where the underestimate of wind speeds near the surface increases as RMW decreases. The modeled and observed wind speeds were grouped into height bins of 10–50, 50–100, 100–200, 200–300, 300–400, 400–500, 500–700, and 700–1000 m.

Figure 10 presents a comparison of the modeled and observed ratios of U_{10}/U_{max} plotted versus U_{max} for dropsonde data collected around the RMW. The observed values of U_{10}/U_{max} are obtained by extending the log-law velocity profiles to the 10-m level using the LSF

results computed over the three different height ranges discussed earlier. The mean value of U_{10}/U_{max} obtained from the model is 0.716. The mean values of U_{10}/U_{max} computed from the data using a LSF over height ranges of 20–200, 20–150, and 20–100 m are 0.703, 0.713, and 0.719, respectively. The corresponding R^2 values are 0.32, 0.57, and 0.65, respectively. The mean modeled value of U_{10}/\bar{U}_{500} (where \bar{U}_{500} is the wind speed averaged over the lower 500 m of the boundary layer) is 0.755, which is slightly lower than the value of 0.78 reported in Powell et al. (2003).

Figure 11 presents the variation of the mean and CoV of error with height for the outside RMW cases. It is seen that in all the cases the mean error is less than 5%. Outside of the RMW, the mean ratios of U_{10}/U_{max} for the observed and the modeled wind speeds are 0.698 and 0.686, respectively, implying a mean underestimate of the surface-level wind speeds of about 2%.

The empirical hurricane boundary layer model described here is shown to be able to reasonably well reproduce the shape of the marine hurricane boundary

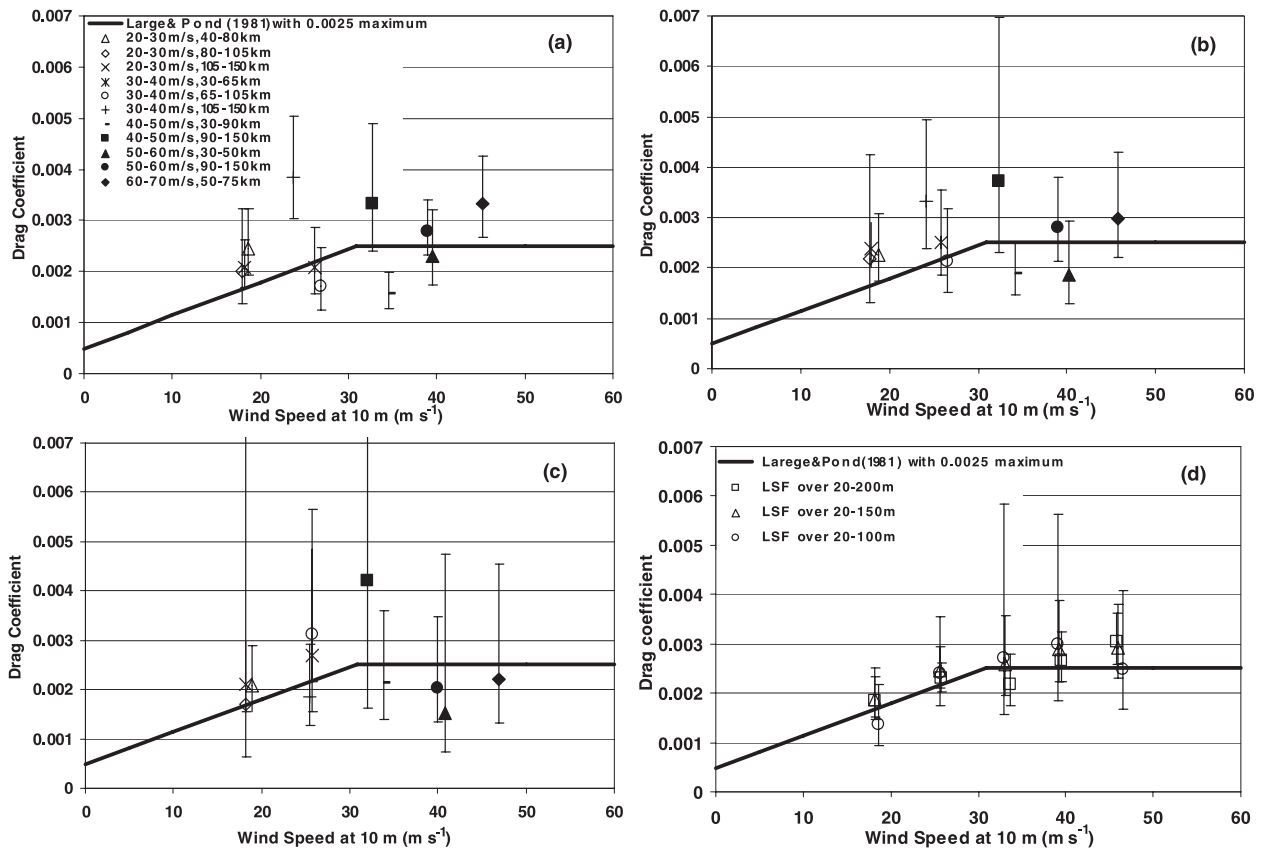


FIG. 5. Variation of the sea surface drag coefficient with mean wind speed at 10 m, outside-RMW case: least squares fit for a height range of (a) 20–200, (b) 20–150, (c) 20–100 m, and (d) no separation by radius.

layer given only a wind speed at gradient or jet height, and a distance r from the center of the storm. The height of the jet is adequately described using a simple model where the jet height is inversely proportional to either, I or \sqrt{I} . This radial variation of jet height and existence of a low-level jet has also been verified by Kepert (2006a,b). Because of the limitation of the number of available vertical profiles of horizontal wind speed, there was insufficient data to further separate the profiles by azimuth in addition to both wind speed and radius bins. As a result, any variation in the jet height as a function of azimuth [as is indicated by Kepert (2001)] is lost in the hurricane boundary layer model presented here. However, the magnitude of the jet strength and its variation with azimuth is modeled using the slab model representation of the hurricane wind field, as described later.

4. Sea-land transition

The characteristics of the hurricane boundary layer described previously are representative of open water (marine) conditions and not for the overland case. Over

land there is virtually no dropsonde data to determine the characteristics of the overland hurricane boundary layer. The approach taken here to model the sea-land transition follows the classical approach (e.g., Deaves 1981; Kao et al. 1974), where the wind speed at the top of the boundary layer is assumed to remain unchanged as the flow moves over a new roughness regime. As was shown for the marine boundary layer, the variation of the horizontal wind speed with height near the surface is controlled by the surface roughness only as described by the log law, and we assume the same applies for hurricane winds over land, consistent with, for example, Powell et al. (1996). The shape of the mean boundary layer over land is therefore assumed to be adequately represented by Eq. (5) and the methodology outlined in Kepert (2001) is used to estimate the increase in the boundary layer height associated with a change in surface roughness.

The increase in the boundary layer height, H is modeled using Eq. (6), which requires an estimate of the increase in K as a function of the increase in C_d . For estimating the increase in the value of K as the wind moves from sea to land (open terrain), K is taken as

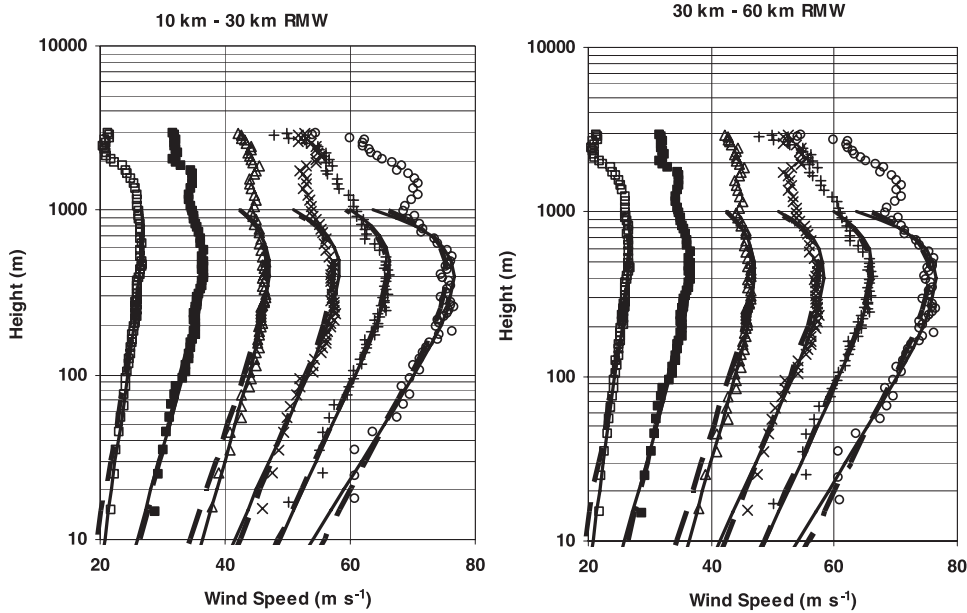


FIG. 6. Observed and modeled wind speed profiles for the (left) 10–30- and (right) 30–60-km RMW cases. Solid lines represent model data derived using least squares fit values of surface roughness and friction velocity using LSF over 20–200-m range. Dashed lines represent model results using C_d derived from truncated Large and Pond (1981) drag coefficient model.

$$K \approx \frac{C_d U^2}{\partial U / \partial z} = \frac{u_*^2}{\partial U / \partial z} \approx k z u_* \tag{8}$$

where k is the von Kármán coefficient.

Equations (6) and (8) are used to estimate the increase in H , yielding typical estimates of the increase in H ranging between 20% and 30% for land defined with $z_0 = 0.03$ m, with the magnitude of the increase varying

with both wind speed and radius. The value of H computed using Eqs. (6) and (8) is dependent on the value of z used in Eq. (8), but the ratio of the two boundary layer heights is for practical purposes independent of the value of z used in Eq. (8).

Figure 12 presents the ratio of the modeled mean wind speed over land ($z_0 = 0.03$ m) to the mean wind speed over water ($z_0 = 0.0013$ m) as a function of the

TABLE 6. Hurricane boundary layer model parameters inside RMW.

RMW (km)	MBL (m s ⁻¹)	Boundary layer model parameters obtained using method 1 (20–200-m LSF values)					Boundary layer model parameters obtained using method 2				
		U_{10} (m s ⁻¹)	C_d	z_0 (m)	H^* (m)	R^2	U_{10} (m s ⁻¹)	C_d	z_0 (m)	H^* (m)	R^2
10–30	20–29	20.7	0.0010	0.0000	650	0.98	19.5	0.0018	0.0007	520	0.93
10–30	30–39	25.9	0.0024	0.0029	440	0.97	26.5	0.0019	0.0010	460	0.98
10–30	40–49	36.3	0.0013	0.0002	380	0.92	34.5	0.0019	0.0010	400	0.82
10–30	50–59	41.5	0.0025	0.0032	380	0.91	42.5	0.0019	0.0010	375	0.93
10–30	60–69	48.9	0.0019	0.0009	400	0.93	48.7	0.0019	0.0010	390	0.94
10–30	70–85	54.1	0.0028	0.0049	350	0.90	56.0	0.0019	0.0010	370	0.92
30–60	20–29	19.5	0.0018	0.0009	650	0.98	19.5	0.0018	0.0007	675	0.98
30–60	30–39	26.2	0.0021	0.0016	600	0.96	26.4	0.0022	0.0020	480	0.99
30–60	40–49	32.9	0.0025	0.0033	550	0.99	33.5	0.0022	0.0020	510	0.98
30–60	50–59	39.3	0.0026	0.0041	550	0.97	40.8	0.0022	0.0020	480	0.95
30–60	60–69	49.7	0.0017	0.0005	550	0.96	48.0	0.0022	0.0020	500	0.94
30–60	70–85	51.0	0.0033	0.0093	700	0.89	55.0	0.0022	0.0020	550	0.95
60–100	20–29	19.5	0.0018	0.0009	1000	0.98	19.7	0.0018	0.0007	1000	0.98
60–100	30–39	26.8	0.0022	0.0021	750	0.95	27.0	0.0022	0.0022	750	0.97
60–100	40–49	32.9	0.0021	0.0015	900	0.95	33.0	0.0025	0.0034	700	0.97
60–100	50–59	38.0	0.0026	0.0042	800	0.95	38.9	0.0025	0.0034	675	0.96

TABLE 7. Hurricane boundary layer model parameters outside RMW.

Radius (km)	MBL (m s ⁻¹)	Boundary layer model parameters obtained using method 1 (20–200-m LSF values)					Boundary layer model parameters obtained using method 2				
		<i>U</i> ₁₀ (m s ⁻¹)	<i>C</i> _d	<i>z</i> ₀ (m)	<i>H</i> * (m)	<i>R</i> ²	<i>U</i> ₁₀ (m s ⁻¹)	<i>C</i> _d	<i>z</i> ₀ (m)	<i>H</i> * (m)	<i>R</i> ²
40–80	20–29	18.6	0.0025	0.0031	470	0.91	19.1	0.0017	0.0007	570	0.95
85–105	20–29	17.9	0.0020	0.0014	900	0.99	18.4	0.0017	0.0006	970	0.99
105–150	20–29	18.2	0.0021	0.0015	1250	0.99	18.7	0.0017	0.0006	1170	0.98
30–65	30–39	26.2	0.0021	0.0015	460	0.99	25.9	0.0022	0.0019	480	0.99
65–105	30–39	26.9	0.0017	0.0006	570	0.99	26.3	0.0022	0.0020	570	0.99
105–150	30–39	23.8	0.0038	0.0158	580	0.99	25.7	0.0022	0.0018	760	0.98
30–90	40–49	34.6	0.0016	0.0004	670	0.99	33.2	0.0025	0.0034	490	0.99
90–150	40–49	32.7	0.0033	0.0097	520	0.99	33.7	0.0025	0.0034	570	0.99
30–50	50–59	39.5	0.0023	0.0024	420	0.99	39.0	0.0025	0.0034	440	0.99
50–150	50–59	39.0	0.0028	0.0051	410	0.99	39.3	0.0025	0.0034	460	0.99
50–75	60–69	45.2	0.0033	0.0098	490	0.98	46.9	0.0025	0.0034	500	0.98

marine boundary layer height. Also shown in Fig. 12 is the wind speed ratio computed using the Engineering Science and Data Unit (ESDU; 1982) transition model. Figure 12 shows that the reduction of the mean wind speed as the wind moves from the sea to the land associated with a hurricane is less than that estimated using the ESDU model, and that the wind speed reduction factor is dependent on *H*, and hence storm intensity and size. The wind speed reduction factors given in Fig. 12 are larger (larger factors correspond to a smaller reduction in wind speed) than those predicted by ESDU for large *H* but match the model given in Simiu and Scanlan (1996) for large *H*. In the model implementation, the increase in the boundary layer height predicted using Eqs. (6) and (8) is further increased so that the resulting reduction in

the wind speed associated with the sea land transition matches that given in ESDU (1982) for large *H*. Using this approach for typical values of *H* (~600 m) near the RMW, the predicted reduction in the mean wind speed matched that given by the model given in Simiu and Scanlan (1996). The wind speed reduction factors shown in Fig. 12 are representative of a fully transitioned boundary layer.

As the wind moves from the sea to land, the value of the maximum wind speed at a given height in the new rougher terrain approaches the fully transitioned value asymptotically over some fetch distance *F*. Published estimates of the fetch length vary markedly, ranging from a few kilometers (e.g., W. H. Melbourne 1992, personal communication) to in excess of 100 km (ESDU 1982; Deaves 1981). Powell et al. (1996) suggest that

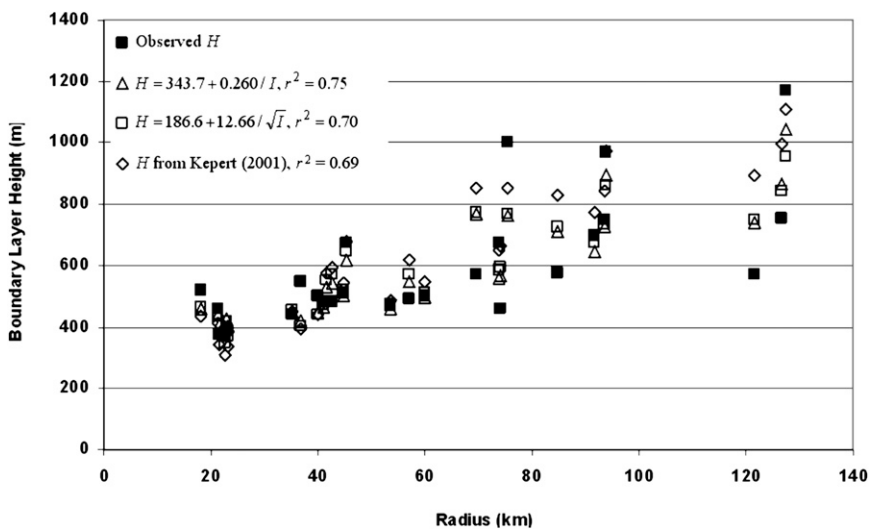


FIG. 7. Comparison of regression model, Kepert (2001) model, and observed boundary layer heights.

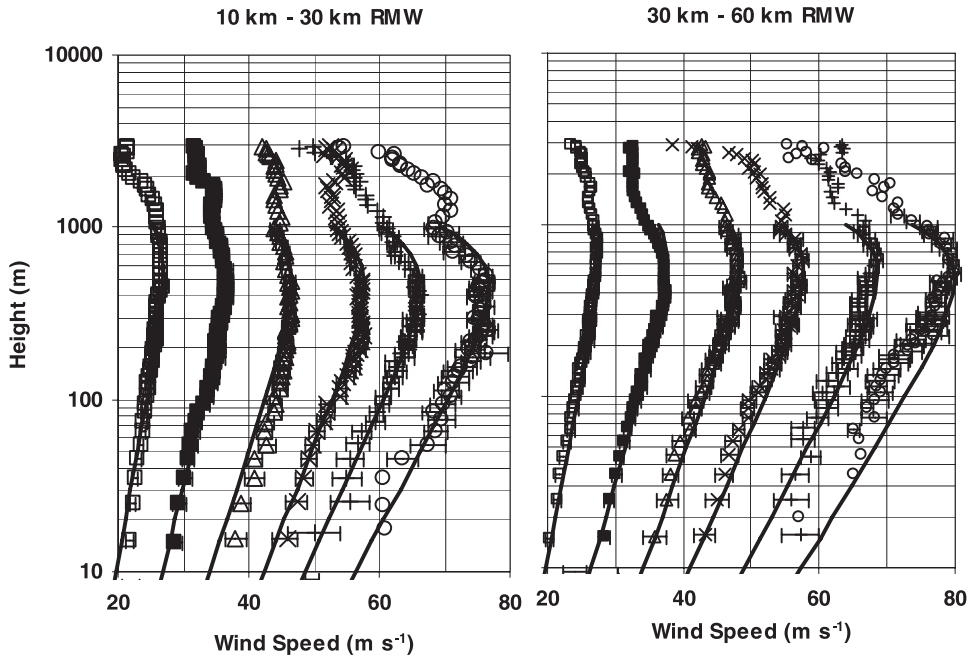


FIG. 8. Observed and modeled wind speed profiles near the RMW for the (left) 10–30- and (right) 30–60-km RMW cases. Solid lines represent model wind speeds computed given U_{max} , RMW, and f . Horizontal error bars represent the 95th percentile error on the estimate of the mean wind speed.

wind measurements at a height of 10 m taken as far as 20–30 km inland are still influenced by the upstream marine roughness. For modeling the transition from sea to land, the ESDU model is used but the limiting fetch distance is reduced to 20 km from the ~ 100 km used in ESDU (1982). The use of the smaller fetch distance is consistent with the lower boundary layer heights associated with tropical cyclones (~ 600 m) as compared with much larger values (~ 3000 m) used in ESDU where H scales as u_* / f rather than $\sqrt{2Kl}$.

The ESDU transition model was chosen since it provides a means to transition the wind speeds associated with an arbitrary averaging time (i.e., hourly mean, 10-min mean, peak gust, etc.). Figure 13 shows a comparison of the original and modified ESDU transition functions for the gust and hourly mean wind speeds. In either model, it is evident that at a distance of about 1 km approximately 60% of the transition (or wind speed reduction) has already occurred. An exact value of F is considered to be difficult, if not impossible to

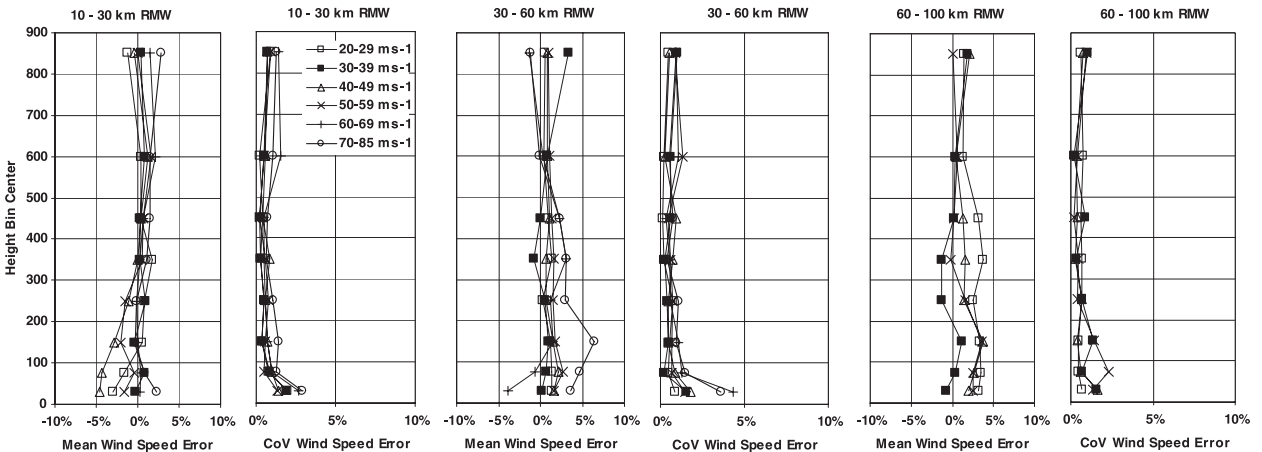


FIG. 9. Mean and CoV of error (defined as modeled – observed) in modeled wind speeds vs height for dropsonde data taken near RMW.

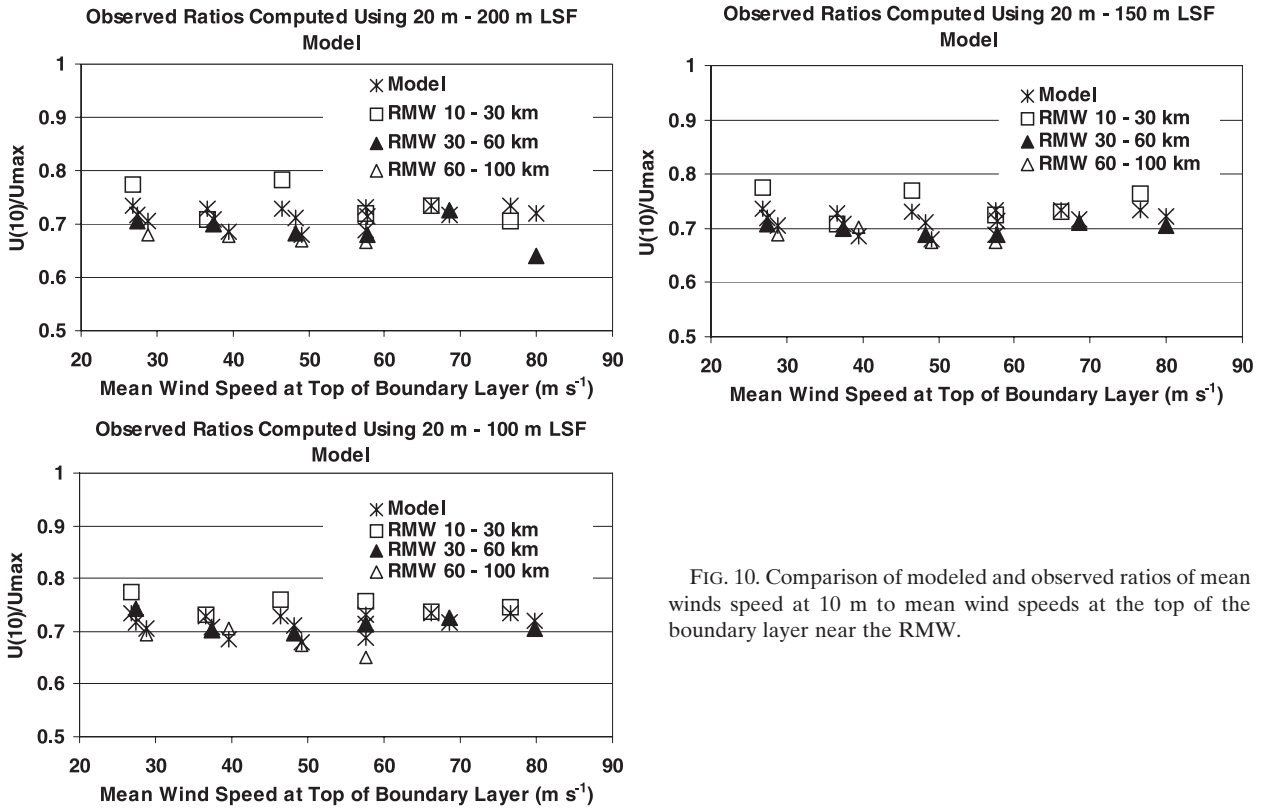


FIG. 10. Comparison of modeled and observed ratios of mean winds speed at 10 m to mean wind speeds at the top of the boundary layer near the RMW.

verify, and an inspection of Fig. 13 indicates that the error in the predicted wind speed is not particularly sensitive to the exact value of F (for $F > 10$ km). For example, the difference between the model estimates of the degree to which the wind speed has reached

equilibrium at 10 km [approximately where the difference between the ESDU, ($F \sim 100$ km) and the modified ESDU, ($F = 20$ km) function reaches a maximum] is about 10%. Referring to Fig. 12 it is seen that the maximum reduction in the mean wind speed

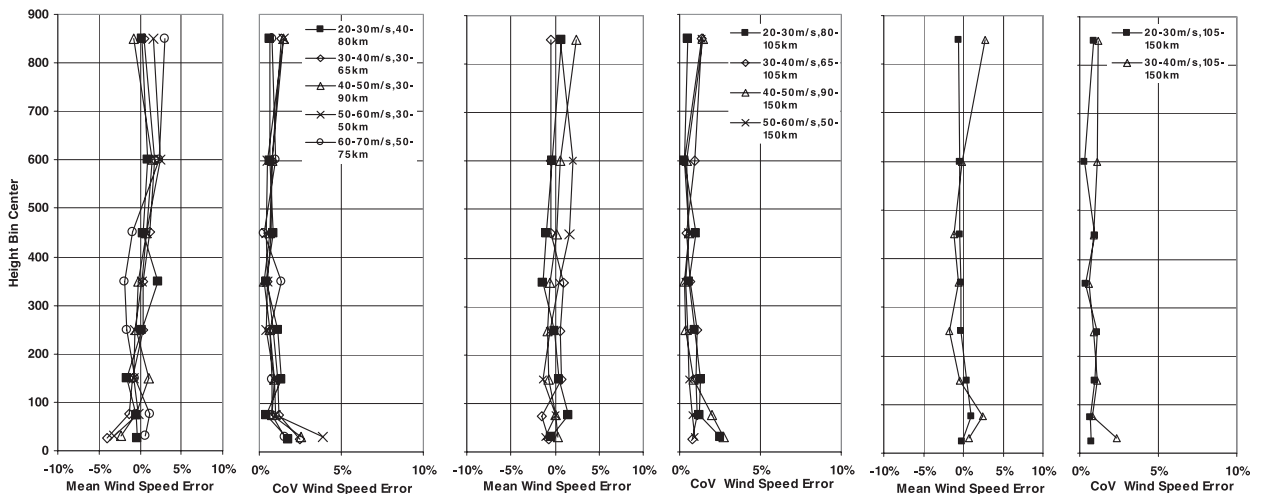


FIG. 11. As in Fig. 9, but for data taken outside RMW region.

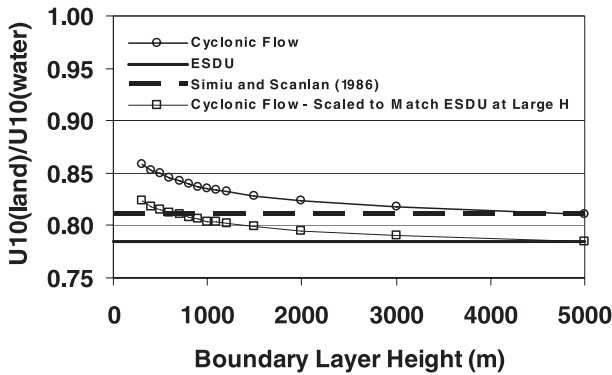


FIG. 12. Ratio of the fully transitioned modeled mean wind speed over land ($z_0 = 0.03$ m) to the modeled mean wind speed over water ($z_0 = 0.0013$ m) as a function of boundary layer height.

using the ESDU model is about 17%, thus the magnitude of the wind speed error associated with the assumed fetch length at this location is about 10% of 17%, or $\sim 1.7\%$.

5. Model verification

Verification of the boundary layer model as a whole, with an emphasis on the sea–land transition, is made difficult because of the paucity of measurements of both marine and nearby overland wind speeds in landfalling hurricanes. Furthermore, experimental verification of the results suggest that the reduction in wind speed associated with the change in roughness from sea to land is less than what is expected in noncyclonic winds is complicated by the fact that the reduction in wind speed as a function of distance inland includes the combined effects of the transition model and the wind speed reduction model.

The approach taken here to verify the combined boundary layer-transition model uses comparisons of time series of measured mean and gust wind speeds combined with model estimates of mean and gust wind speeds. The model wind speed estimates are made using a slab representation of the horizontal structure of a

hurricane boundary layer coupled with the 2D wind speed profile and terrain transition models. In addition to comparisons of modeled and observed wind speeds using the models described herein, we also perform comparisons of modeled and observed surface wind speeds using the Holland wind field model (Holland 1980) coupled with a constant wind speed reduction factor.

Details of the slab model approach are given in Thompson and Cardone (1996) and Vickery et al. (2000), but a brief overview of the slab model implementation is presented here. The model solves the depth-averaged dry equations of horizontal motion forced by a constant translating pressure field. A finite difference scheme is used to solve for the steady-state wind field over a set of nested rectangular grids. The basis of this approach is the assumption that the large-scale structure of the hurricane wind field changes relatively slowly over time. Therefore, at any instant the wind field may be considered to be very nearly at the steady-state conditions that it would be if it were moving over homogeneous terrain at a constant translational speed equivalent to the instantaneous translational speed.

The slab model is based on a formulation originally developed by Chow (1971) and is similar to the model given in Thompson and Cardone (1996) but is simplified using the Fourier series approach described in Vickery et al. (2000). The equation of horizontal motion, vertically averaged through the height of the boundary layer, is written in earth fixed coordinates as

$$\frac{d\mathbf{V}}{dt} + f|\mathbf{k} \times \mathbf{V}| = -\frac{1}{\rho}\nabla p + \nabla \cdot (K_H \nabla \mathbf{V}) - \frac{C_d}{h}|\mathbf{V}|\mathbf{V}, \tag{9a}$$

where

$$\frac{d}{dt} = \frac{\partial}{\partial t} + \mathbf{V} \cdot \nabla. \tag{9b}$$

Here \mathbf{V} is the vertically averaged horizontal velocity, f is the Coriolis parameter, \mathbf{k} is the unit vector in the vertical direction, ρ is the air density, K_H is the horizontal

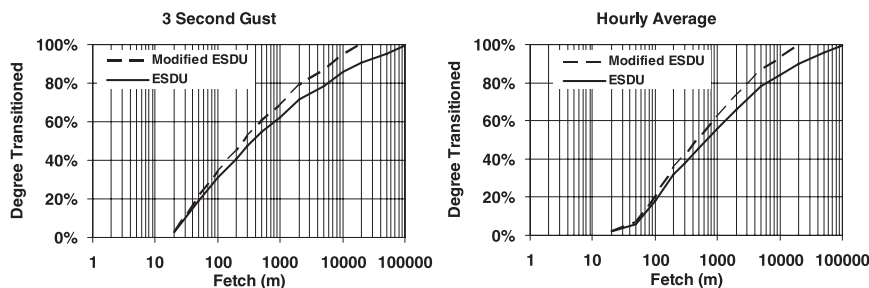


FIG. 13. ESDU and modified ESDU wind speed transition functions at 10-m elevation.

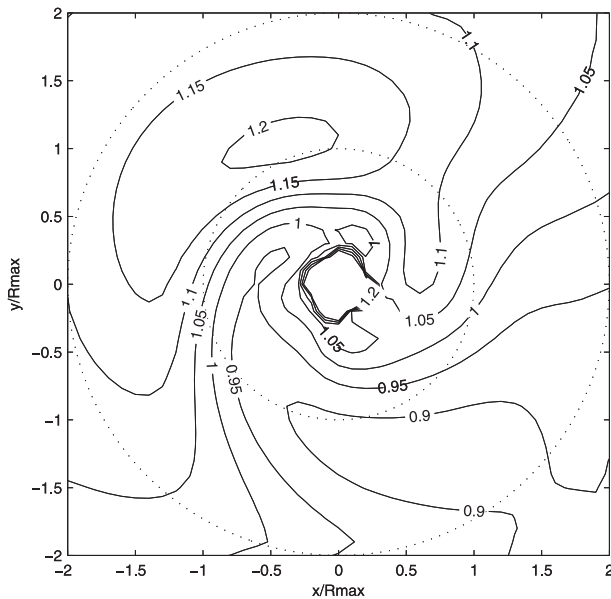


FIG. 14. Jet strength, defined as the depth average wind speed divided by the gradient balance wind speed, computed using the slab model for a hurricane moving toward the top of the page.

eddy viscosity coefficient, C_d is the drag coefficient, and h is the height of the hurricane boundary layer, taken as constant and equal to 1000 m. It is assumed that the vertical advection of momentum is small relative to the horizontal advection of momentum and is ignored.

The pressure gradients dp/dx and dp/dy are prescribed by transforming the following expression for the radial pressure gradient:

$$\frac{\partial p}{\partial r} = \frac{\Delta p B}{r} \left(\frac{\text{RMW}}{r} \right)^B \exp \left[- \left[\frac{\text{RMW}}{r} \right]^B \right], \quad (10)$$

where B is Holland's (1980) radial pressure profile parameter, RMW is the radius to maximum winds, r is the distance from the center of the hurricane, and Δp is the central pressure difference. Inputs to the slab model are the pressure gradients (dp/dx and dp/dy), the surface drag coefficient C_d , and the storm's translational velocity (u_c, v_c). For the overwater case, the drag coefficient is modeled using the truncated version of model described by Large and Pond (1981). In the overland case, C_d is modeled as constant and equal to 0.0047 (open terrain). The solution to the equations of motion is evolved to the steady-state wind field solution by integrating forward until the acceleration is acceptably small. A nested grid system composed of six concentric rectangular grids is used to solve for the steady-state

wind field using a finite difference approach. Each grid is composed of the same number of nodes, but the internode distance is halved with each successive grid. The smallest grid size is set as 10% of the RMW of the storm being simulated. Since it is the storm-centered velocity \mathbf{V}_s that has been calculated, the storm translational velocity \mathbf{V}_c , is added on to the results to get the earth-centered velocity field.

As described in Vickery et al. (2000) the model uses precomputed solutions to Eq. (9) coupled with an interpolation approach to arrive at a solution for the vertically averaged horizontal wind speed for a given set of hurricane parameters. To cover the full range of possible combinations of central pressure, RMW, and so on, the wind fields for 14 040 tropical cyclones were precomputed, for each of 9 values of B , 13 values of RMW, 12 values of Δp , and 10 values of translation speed. One complete set of hurricanes is generated for the overwater case, and another set for the overland case. For each storm, cubic splines fitted along the x and y directions are used to interpolate u and v components at points around circular paths concentric with the grid center. These are then transformed into Fourier series with the Fourier coefficients saved to disk and recalled as needed for modeling a given storm. For each modeled storm, the velocities u and v at some location x and y are obtained through a combination of interpolation and scaling from the results stored on disk.

In the use of the slab model, the resulting integrated wind speed (mean value throughout the boundary layer) is adjusted to be representative of the maximum wind speed in the boundary layer. The difference between the maximum wind speed and the depth-averaged wind speed is only a few percent, and varies dependent upon whether averaging is performed over the assumed 1000-m boundary layer height used in the slab model, or if the averaging height is the modeled boundary layer depth (jet height). In the comparisons of modeled and observed marine and land wind speeds, an additional 2% increase in the modeled winds was introduced to eliminate a low overall bias in the comparisons of modeled and observed wind speeds.

The slab model approach to modeling the hurricane wind field brings out features that are not reproduced in simple gradient balance vortex models or empirical models, such as those described in Schwerdt et al. (1979) or Holland (1980). For example, Fig. 14 presents the distribution and magnitude of the jet determined (here defined as the depth-averaged wind speed divided by the gradient balance wind speed) using the slab model. A comparison of the jet strength and its variation with azimuth resulting from the 2D slab model with the results of a full 3D model of a translating hurricane as

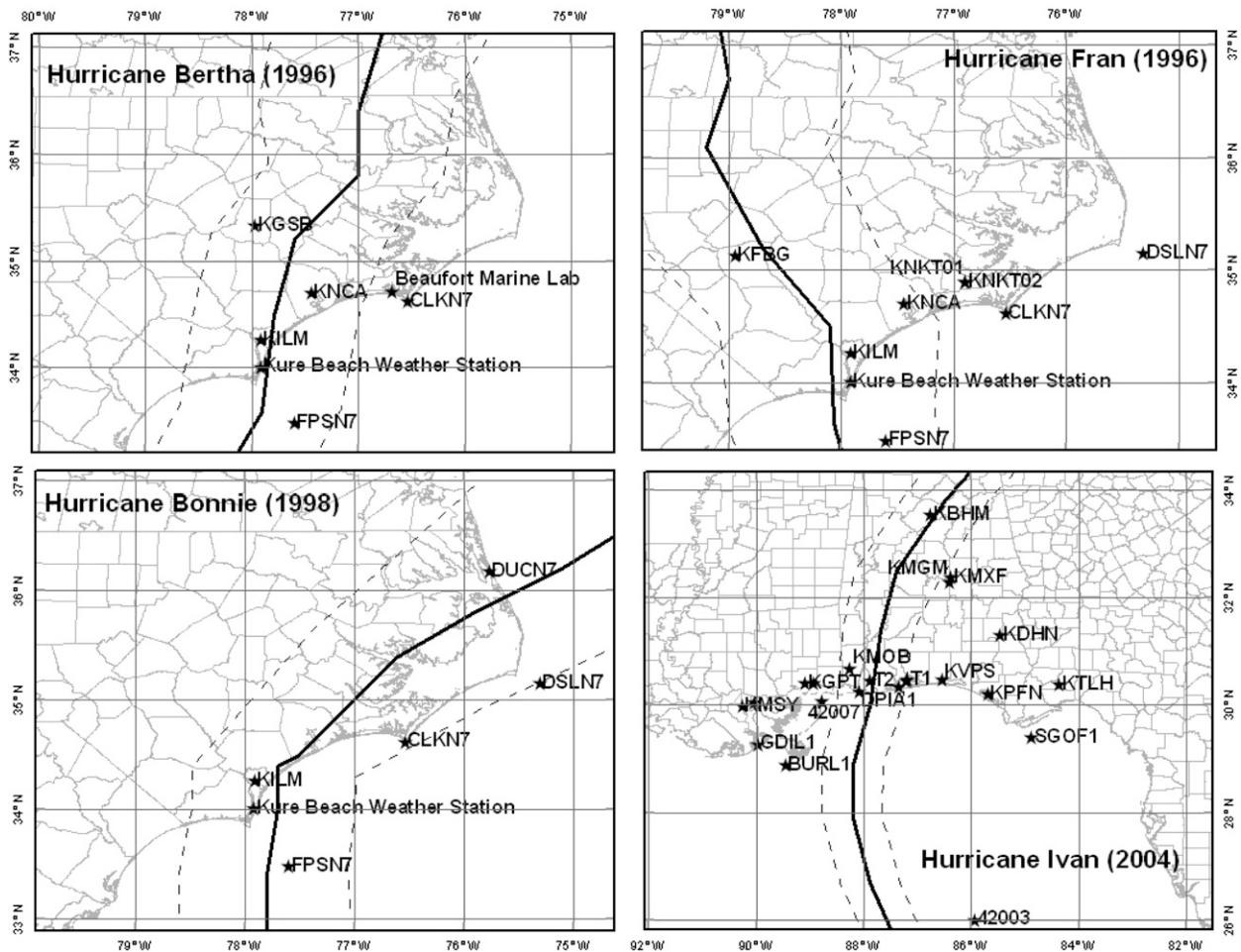


FIG. 15. Tracks of hurricanes showing locations of marine- and land-based anemometers. Dashed lines represent approximate lateral extent of the RMW.

presented in Kepert and Wang (2001) indicate that the 2D numerical slab model is able to produce a horizontal variation of the magnitude of the jet characteristics corresponding to a height of ~500 m that are similar to those produced by a full 3D numerical model. However, the slab model yields an area of slightly subgradient wind speeds in the right rear quadrant of the hurricane that does not appear in the 3D model results. Furthermore, the variation of the jet height with azimuth is not provided using the slab model.

In the verification of the model with an emphasis on the sea-land transition, only hurricanes having continuous measurements of wind speeds both over land and over water near the landfall location are useful. The only reasonably well documented hurricanes that meet this criterion include Hurricanes Bertha and Fran (1996), and Hurricane Bonnie (1999), near the North Carolina coast, and Hurricane Ivan (2004) along the Gulf Coast. The validation approach is indirect, with the

process involving a comparison of modeled and observed maximum peak gust wind speeds produced by the hurricanes over both marine and land terrains. Conclusions as to the validity of the model are inferred by determining if there is a bias in the estimates of the modeled marine winds versus the modeled overland winds. Figure 15 shows the tracks of the four hurricanes, the lateral extent of the RMW, and the locations of the anemometers used in the validation process. All measured gust wind speeds have been adjusted to be representative of 3-s gust speeds at a height of 10 m, in either open terrain ($z_0 = 0.03$ m) or marine conditions. In the case of marine wind speed measurements obtained from 3-m discus buoys, the measured wind speeds in high wind cases have been increased by 10% to account for the underestimates in the measured wind speeds as described in Gilhousen (2006).

Each hurricane is modeled using information on the hurricane track (position and central pressure) obtained

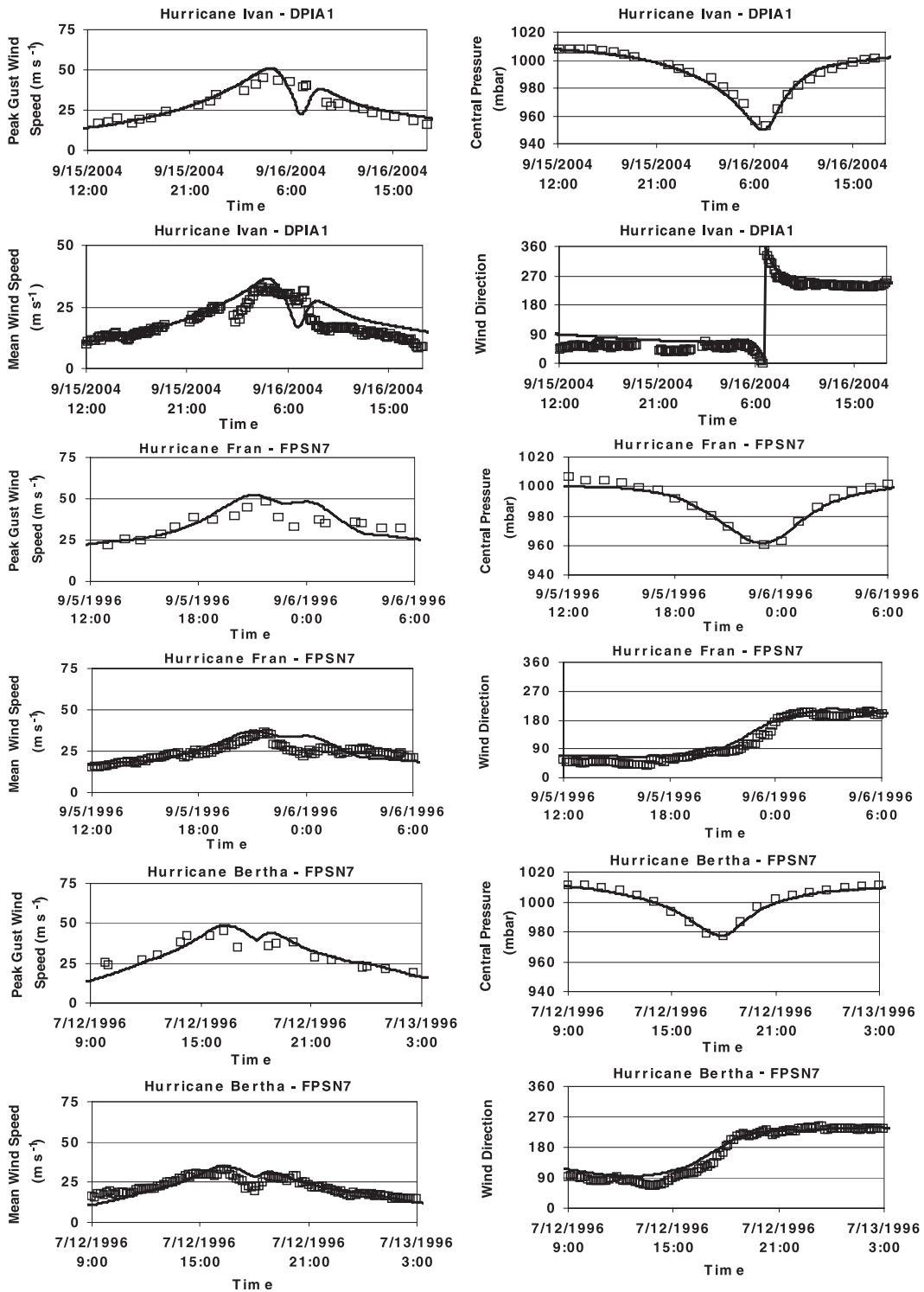


FIG. 16. Example plots showing modeled and observed wind speeds, surface pressures, and wind directions. Model results are represented by the solid lines; observed values are represented by the open squares.

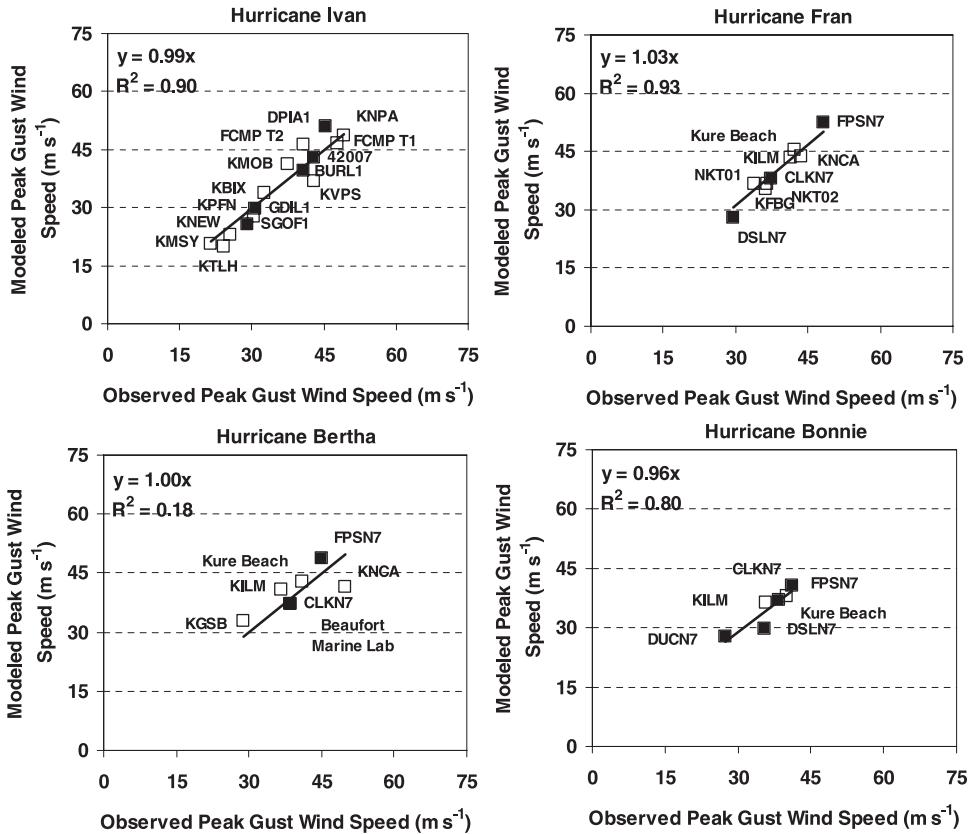


FIG. 17. Comparisons of modeled and observed peak gust wind speeds for land- and marine-based stations (separated by storm). Open squares represent land-based measurements; solid squares represent marine-based measurements. All wind speeds are at a height of 10 m in either open terrain or for marine conditions.

from the National Hurricane Center, coupled with estimates of the RMW and the Holland B parameter (Holland 1980). The modeled pressure field is axisymmetric, but varies with time. The initial estimate of the

RMW is usually obtained from H^* Wind snapshots of the hurricane wind field at or near the time of landfall. The final estimates of B and the RMW and their variation with time after landfall are obtained through an

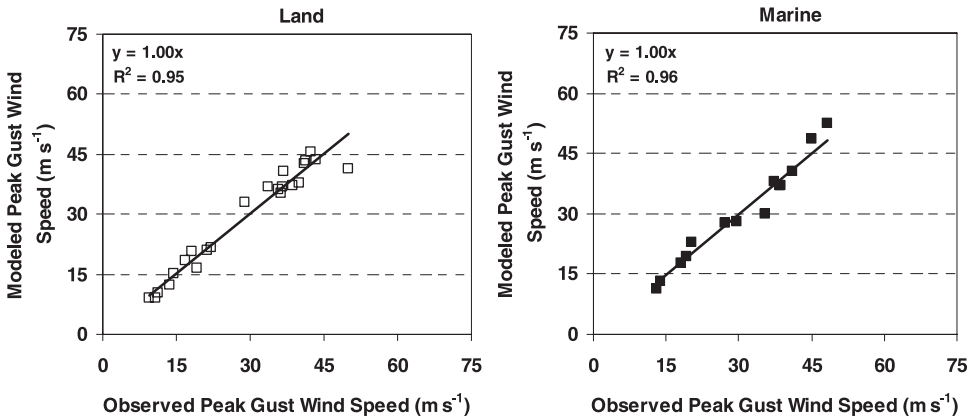


FIG. 18. Summary comparison of modeled and observed peak gust wind speeds for (left) land- and (right) marine-based stations (separated by terrain).

TABLE 8. Number of wind speed records for each hurricane.

Year	Hurricane name	Number of complete wind speed records			Number of complete wind speed records	
		Land	Marine	Total	Inside RMW	Outside RMW
1979	Frederic	4		4	2	2
1985	Elena	3	2	5	2	3
1989	Hugo	6	1	7	5	2
1991	Bob	2	5	7	4	3
1992	Andrew	1	2	3	1	2
1993	Emily		9	9	4	5
1995	Erin	5	2	7	5	2
1995	Opal	5	2	7	5	2
1996	Bertha	5	3	8	5	3
1996	Fran	9	3	12	6	6
1998	Bonnie	2	4	6	6	
1998	Georges	3	10	13	8	5
1999	Floyd	2	4	6	4	2
1999	Irene	4	5	9	3	6
2003	Isabel	10	7	17	5	12
2004	Charley	12	1	13	4	9
2004	Frances	13	1	14	9	5
2004	Ivan	15	6	21	7	14
2004	Jeanne	17	2	19	8	11
2005	Dennis	9	3	12	2	10
2005	Katrina	8	2	10	2	8
2005	Ophelia	5	7	12	6	6
2005	Rita	14		14	6	8
2005	Wilma	21	2	23	20	3
	Total	175	83	258	129	129

iterative approach by reproducing the overall shapes of the wind speed and direction traces and surface pressure traces obtained from as many ground stations as possible. Figure 16 presents examples of comparison of wind speed and pressure data obtained from stations located near the point of landfall for different hurricanes. The assignment of RMW and B is performed with the objective of describing the overall shape of the wind speed and pressure time histories, rather than matching the individual station maximum wind speeds. The modeling of the hurricane wind field using a symmetric pressure field is a simplification of real-world hurricanes, which often are characterized by RMW and B values, which vary with both azimuth and radius, but as will be shown later, in most cases, the model provides a reasonably accurate representation of the overall hurricane wind field, particularly in the areas experiencing the strongest winds (i.e., near the RMW). An example of a hurricane

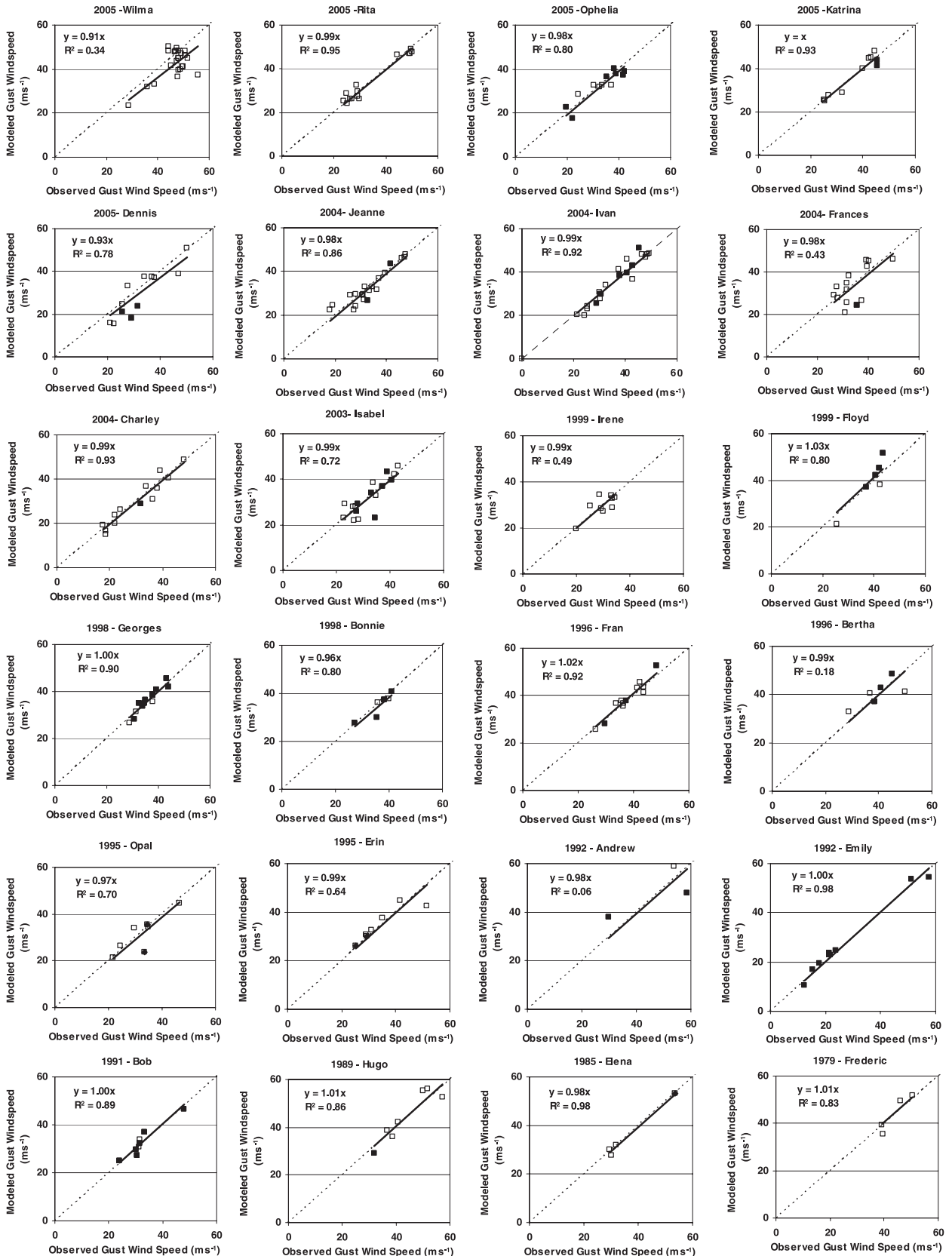
where modeling the wind field with a single value of B and RMW fails to adequately model the surface-level winds is Hurricane Wilma in south Florida.

Figure 17 shows comparisons of the modeled and observed peak gust wind speeds for the four hurricanes noted above, with the overland and overwater wind speeds indicated with different symbols. The comparisons suggest that there is no bias in the modeled wind speeds as compared to the measured wind speeds for either the overland or overwater cases. This lack of bias is further emphasized in Fig. 18, where the comparison is performed with the land and marine wind speed data combined for the four storms, but the comparisons given are separated by terrain type.

An extensive set of validation studies has been performed using the hurricane wind field–boundary layer model described herein through comparisons of modeled and observed wind speed and pressure data obtained for

→

FIG. 19. Comparison of modeled and observed maximum peak gust wind speeds for 24 landfalling hurricanes. Open squares represent land-based measurements; solid squares represent marine-based measurements. All wind speeds are at a height of 10 m in either open terrain or for marine conditions.



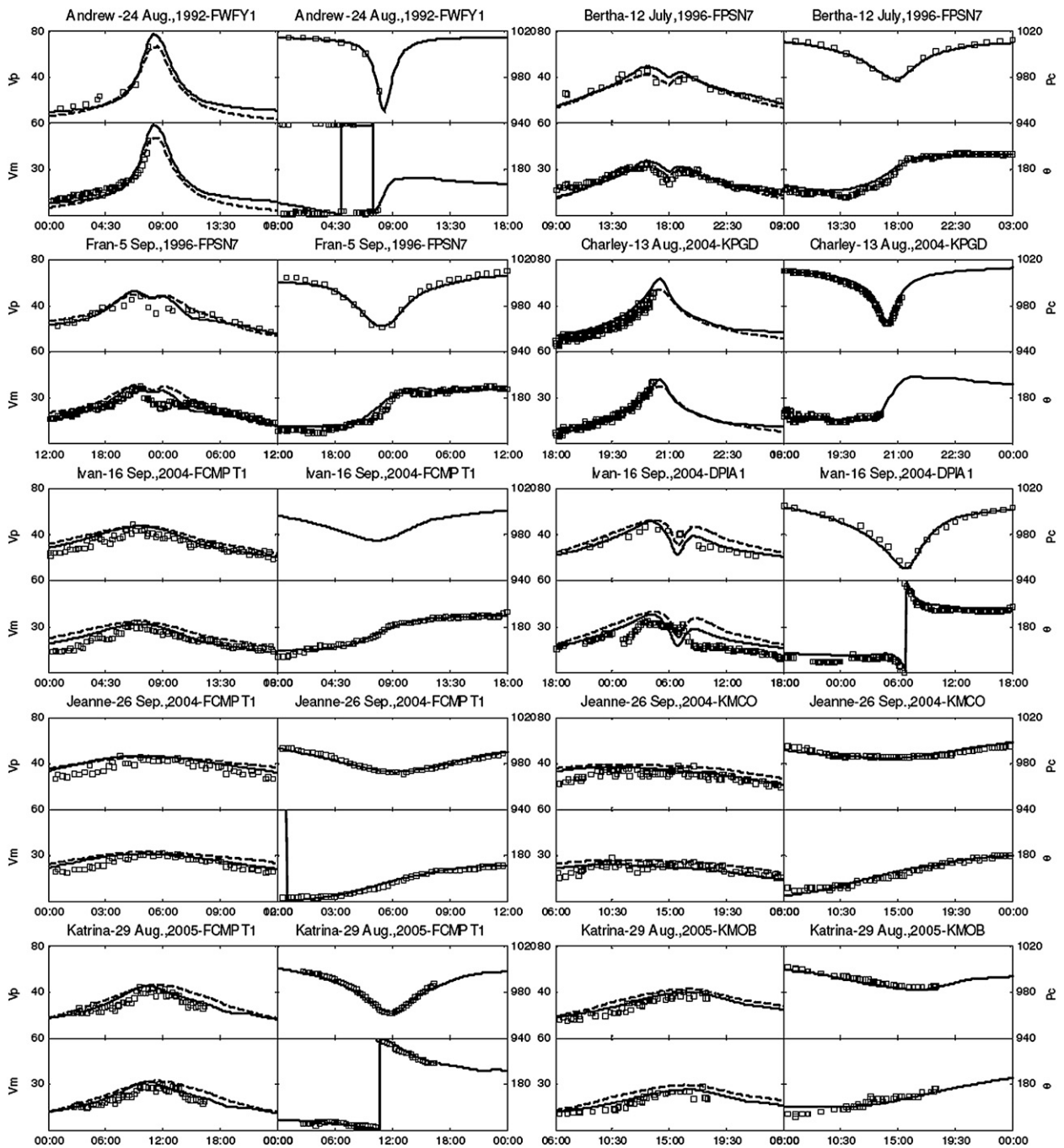


FIG. 20. Similar to Fig. 16. Dashed lines represent model results obtained using the gradient balance equation. Modeled mean wind speed is representative of a 1-h average. Averaging time for observed wind speeds is 10 min at FWYF1, FPSN7, and DPIA1. Averaging time for observed winds at FCMPT1 is 15 min. Averaging times for mean winds at KPGD, KMOB, and KMCO are 2 min.

24 landfalling hurricanes occurring since 1985. In each validation study, estimates of RMW and B , and their variation in time were obtained using the iterative approach described earlier, with the final selection of the values of B and RMW used to define the hurricane

being subjective rather than objective. The number of anemometer stations with either complete continuous records of wind speeds or records of where the maximum wind speed during the storm was measured is given in Table 8. A total of 258 maximum gust wind

TABLE 9. Comparison of regression slope, R^2 , and rms errors of maximum modeled and observed peak gust wind speeds derived using the slab model and a gradient balance model for a hurricane.

Storm name	Gradient balance model with $V_{10}/V_g = 0.85$			Slab model with presented boundary layer model			% reduction in RMSE from gradient balance model
	Slope	R^2	RMSE ($m\ s^{-1}$)	Slope	R^2	RMSE ($m\ s^{-1}$)	
Frederic	0.93	0.87	3.42	1.01	0.83	2.92	15
Elena	1.00	0.96	2.41	0.99	0.99	1.30	46
Hugo	0.92	0.69	5.30	1.01	0.86	3.63	32
Bob	1.08	0.65	4.08	1.01	0.90	2.04	50
Andrew	0.90	-0.02	8.44	0.98	0.06	8.22	3
Emily	0.87	0.91	5.06	1.01	0.98	1.86	63
Erin	0.94	-1.97	5.94	0.99	0.64	3.84	35
Bertha	0.86	-0.11	6.86	1.00	0.18	4.22	38
Fran	1.00	0.85	2.27	1.02	0.93	2.14	6
Opal	1.30	0.73	10.70	0.97	0.70	4.21	61
Bonnie	1.07	0.66	3.55	0.96	0.80	2.49	30
Georges	1.06	0.66	3.85	1.00	0.90	1.63	58
Floyd	1.11	0.70	5.86	1.03	0.80	4.46	24
Irene	1.02	-0.07	3.44	0.99	0.50	3.14	9
Isabel	1.10	0.71	4.86	0.99	0.72	4.05	17
Charley	0.90	0.83	5.17	0.99	0.93	2.78	46
Frances	0.96	0.15	4.98	0.98	0.43	6.28	-26
Ivan	1.02	0.91	2.89	0.99	0.91	2.98	-3
Jeanne	1.05	0.59	3.69	0.98	0.86	3.08	17
Dennis	1.01	0.74	5.28	0.93	0.78	5.62	-6
Katrina	1.07	0.95	3.25	1.00	0.93	2.29	30
Ophelia	0.89	0.72	4.94	0.98	0.80	3.04	38
Rita	1.04	0.66	4.54	0.99	0.95	2.24	51
Wilma	0.94	-0.19	5.99	0.91	0.37	6.71	-12

speeds are included in the data given in Table 8. Table 8 also provides the number of measurement locations that were in or near the RMW and those that were outside the RMW. Note that in many cases, additional incomplete records of wind speeds and pressures were used to assist in estimating the variation in both RMW and B . Figure 19 presents scatterplots summarizing the comparisons of modeled and observed maximum peak gust wind speeds produced by the storms. In each plot, the slope and R^2 values resulting from a linear regression analysis (where the regression line is forced to pass through the origin) are given. In all but one case (Hurricane Wilma), the regression slope is within 4% of unity.

Figure 20 shows 10 example time series of modeled and observed wind speeds, wind directions, and pressures. Modeled wind speeds are given for both the wind field model described herein, and a simple gradient balance wind field model based on Holland's (1980) formulation, with a constant marine surface wind reduction factor (SWRF) equal to 0.85 times the gradient balance solution. In the examples given in Fig. 20, it is seen that the simple gradient balance model tends to underestimate the peak winds (see Andrew FYWF1 and Charley KPGD comparisons), or if the

maximum winds are matched, the gradient balance model overestimates the wind speeds away from the maximum. The factor of 0.85 used in the gradient balance model was chosen through trial and error through comparisons of modeled and observed maximum gust wind speeds from the 258 full-scale anemometer data. The large SWRF of 0.85 (as compared with ~ 0.72 derived from the dropsonde data) is consistent with other high values in the range of 0.8–0.9 appearing in the literature [e.g., Schwerdt et al. (1979; SWRF = 0.95), Batts et al. (1980; SWRF = 0.865), and Georgiou et al. (1983; SWRF = 0.65–0.85)]. The need for a large surface wind reduction factor with a simple gradient balance type windfield model appears to be required to compensate for the lack of supergradient winds produced by these models. The ability of a gradient balance model to match the observed surface winds could be improved by using a SWRF that varies with radius to better compensate for the inability of the model to produce the supergradient winds. Table 9 summarizes the regression slopes, R^2 values and root-mean-square (rms) errors derived from the maximum modeled and observed peak gust wind speeds for both the model described herein and the simple gradient balance model. The results indicate that, in 21 of the 24

hurricanes, the use of the more complex model decreases the rms error. The overall decrease in the peak gust wind speed error is 1.3 m s^{-1} (a 27% decrease in the rms error). In the three cases where the rms error increases, both models performed poorly, with the poor performance arising from a wind field too complex to be modeled with single values of B and RMW.

6. Summary

A hurricane boundary layer model was developed using a combination of mean wind speed profiles computed using dropsonde data and variation of a simplified linear theoretical hurricane boundary layer model described in Kepert (2001). The final hurricane boundary layer model incorporates a combined logarithmic–quadratic variation of the mean wind speed with height. The model replicates the height of the low-level jet observed in the hurricane boundary layer and reproduces the shape of the hurricane boundary layer over the lower 1000 m. The analysis of the vertical profiles of the mean horizontal wind speed from dropsonde data reproduces the observations noted in Powell et al. (2003) that the sea surface drag coefficient reaches a maximum value. The results also suggest that the magnitude of this maximum value decreases with decreasing storm RMW. It is hypothesized that this radius effect may be due to more sea spray being generated from the shorter waves generated within small-radii hurricanes.

A simple linear regression model is used to determine the depth of the boundary layer, which, as predicted by Kepert (2001), decreases with an increase in the inertial stability parameter. The change in the height of the boundary layer as the wind moves from the sea to the land was modeled using the approach outlined in Kepert (2001), and is coupled with a traditional approach to model the reduction in the wind speed from sea to land. The results suggest that the reduction in the wind speed associated with the sea–land transition varies with the height of the hurricane boundary layer, and consequently varies with storm size and intensity because of the relationship between the boundary layer height and the inertial stability parameter.

The hurricane boundary layer model was coupled with a slab representation of a hurricane and then validated through comparisons of modeled and observed peak gust wind speeds measured at both open water and overland locations. The comparisons suggest that the model adequately reproduces the key characteristics of the hurricane boundary layer and the transition from sea to land, but clearly more research is required into the reduction in the surface-level wind speeds as the wind moves from the water to the land. In future hurricanes, as additional

measurements are obtained, by including data from the surface anemometers and near-surface measurements from fixed and mobile radar platforms, the modeling of the sea–land transition may be improved.

REFERENCES

- Batts, M. E., M. R. Cordes, L. R. Russell, J. R. Shaver, and E. Simiu, 1980: Hurricane wind speeds in the United States. National Bureau of Standards, Tech. Rep. BSS-124, U.S. Department of Commerce, 50 pp.
- Bye, J. A. T., and A. D. Jenkins, 2006: Drag coefficient reduction at very high wind speeds. *J. Geophys. Res.*, **111**, C03024, doi: 10.1029/2005JC003114.
- Chow, S. H., 1971: A study of wind field in the planetary boundary layer of a moving tropical cyclone. M.S. thesis, School of Engineering and Science, New York University, 59 pp.
- Deaves, D. M., 1981: Computation of wind flow over changes in surface roughness. *J. Wind Eng. Ind. Aerodyn.*, **7**, 65–94.
- Engineering Sciences Data Unit (ESDU), 1982: Strong winds in the atmospheric boundary layer, Part 1: Mean hourly wind speed. Engineering Sciences Data Unit Item 82026, 63 pp.
- Franklin, J. L., M. L. Black, and K. Valde, 2003: GPS dropwindsonde wind profiles in hurricanes and their operational implications. *Wea. Forecasting*, **18**, 32–44.
- Georgiou, P. N., A. G. Davenport, and B. J. Vickery, Design wind speeds in regions dominated by tropical cyclones. *J. Wind Eng. Ind. Aerodyn.*, **13**, 139–152.
- Gilhouse, D. B., 2006: A complete explanation of why moored buoy winds are less than ship winds. *Mariners Weather Log*, Vol. 50, No. 1, National Weather Service, 4–7.
- Hock, T. R., and J. L. Franklin, 1999: The NCAR GPS dropwindsonde. *Bull. Amer. Meteor. Soc.*, **80**, 407–420.
- Holland, G. J., 1980: An analytical model of wind and pressure profiles in hurricanes. *Mon. Wea. Rev.*, **108**, 1212–1218.
- Kao, K. S., J. C. Wyngaard, and O. R. Cote, 1974: The structure of the two-dimensional internal boundary layer over a sudden change of surface roughness. *J. Atmos. Sci.*, **31**, 738–746.
- Kepert, J. D., 2001: The dynamics of boundary layer jets within the tropical cyclone core. Part I: Linear theory. *J. Atmos. Sci.*, **58**, 2469–2484.
- , 2006a: Observed boundary layer wind structure and balance in the hurricane core. Part I: Hurricane Georges. *J. Atmos. Sci.*, **63**, 2169–2193.
- , 2006b: Observed boundary layer wind structure and balance in the hurricane core. Part II: Hurricane Mitch. *J. Atmos. Sci.*, **63**, 2194–2211.
- , and Y. Wang, 2001: The dynamics of boundary layer jets within the tropical cyclone core. Part II: Non-linear enhancements. *J. Atmos. Sci.*, **58**, 2485–2501.
- Large, W. G., and S. Pond, 1981: Open ocean momentum flux measurements in moderate to strong winds. *J. Phys. Oceanogr.*, **11**, 324–336.
- Makin, V. K., 2005: A note on the drag of the sea surface at hurricane winds. *Bound.-Layer Meteor.*, **115**, 169–176.
- Powell, M. D., S. H. Houston, and T. A. Reinhold, 1996: Hurricane Andrew's landfall in south Florida. Part I: Standardizing measurements for documentation of surface wind fields. *Wea. Forecasting*, **11**, 303–328.
- , —, L. R. Amat, and N. Morisseau-Leroy, 1998: The HRD real-time hurricane wind analysis system. *J. Wind Eng. Ind. Aerodyn.*, **77**, 53–64.

- , P. J. Vickery, and T. A. Reinhold, 2003: Reduced drag coefficients for high wind speeds in tropical cyclones. *Nature*, **422**, 279–283.
- Schwerdt, R. W., F. P. Ho, and R. R. Watkins, 1979: Meteorological criteria for standard project hurricane and probable maximum hurricane wind fields, Gulf and East Coasts of the United States. NOAA Tech. Rep. NWS 23, 317 pp.
- Simiu, E., and R. H. Scanlan, 1996: *Wind Effects on Structures*. 3rd ed. Wiley, 688 pp.
- Thompson, E. F., and V. J. Cardone, 1996: Practical modeling of hurricane surface wind fields. *J. Waterw. Port Coast. Ocean Eng.*, **122**, 195–205.
- Vickery, P. J., P. F. Skerlj, A. C. Steckley, and L. A. Twisdale, 2000: Hurricane wind field model for use in hurricane simulations. *J. Struct. Eng.*, **126**, 1203–1221.